CONTENTS

CHAPTER 3

THE OBSERVATIONS. DATA ANALYSIS AND CALIBRATION

Chapter **3**

THE OBSERVATIONS, DATA ANALYSIS AND CALIBRATION

This chapter discusses the methods of observation, data analysis, and calibration. Section 3.1 discusses the method of observation and the checks on the working of the telescope system using strong point sources. The production of raw maps and the problems (and the solutions adopted) of **CLEANing** large angular scale maps which also contain background radiation are discussed in Section 3.2. The last section discusses the calibration of the data and its repeatability.

3.1 OBSERVATIONS

3.1.1 The 24 hour Observation

All the continuum observations made with GEETEE are meridian transit observations. For the purpose of making the all-sky map, the observation was carried out with a single row of dipoles in the EW arm and the 88 rows in the southern arm (Fig. **2.6(a))**. Time division multiplexing with a cycle time of ≈ 1 **sec** was adopted to accept at any instant of time only one out of every **4** rows in the southern array so that the same transmission line and front end could be used for every set of four rows in the southern array. The 88 complex visibilities were continuously recorded starting at the beginning of every hour. At the end of each ≈ 8 **sec** period a record gap was written on the magnetic tape. Following the record gap that occurs after the 59th minute, the antenna was replaced by the noise diode (section **2.4.2)** and its output recorded for the next three records. At the end of the third record, the noise diode was turned off and the antenna

re-connected.   Recording of the antenna output was started again at the beginning of the next minute. Thus, the last three records in each file contain information on the gains of the last stage amplifiers.   This gap of $\lesssim$ 1 min was filled in   the next 24 hours when the file gaps were arranged to come at the end of every half hour instead of at the end of every hour (this can be set in the magnetic tape interface unit).   Alternatively, the gap can also be filled by interpolating the adjacent data stretches observed on the same day.   This procedure has been found to work well.

The observations presented in this thesis were made during the last **15** days of January, **1987.**   In principle, **any** one continuous day is enough to produce an all sky map. By observing for **15** days one was able to check in detail the repeatability of the data.   `

3.1.2 Observing condition

Observing   conditions   at Gauribidanur   are   critically dependent on solar activity.   Non-solar astronomy is best done during a solar minimum (one of which occurred in **1987).**   During periods of increased solar activity the interference level is so high and continuous that useful observations are not possible during most of the day.   In addition, the ionosphere gets so highly disturbed as to heavily corrugate the wavefronts falling on the antenna. As a result, even over a length of 1.4 km of the EW array the signal gets dephased and the sources can   partially or completely disappear.   This effect occurs only during the night.   The present observations were carried out during a period

when the interference was remarkably low. In fact, in one entire set of **24** hours of data which has gone into the all-sky map, there were only half a dozen places where interference appeared, each lasting for a duration of **< 30 sec** of time. In addition, no dephasing over the antenna was observed during this period indicating that the ionosphere was well-behaved **!**. This can indeed be seen by the results of the analyses done on point source fluxes presented in this chapter.

3.1.3 Point sources as probes of the antenna response

We mentioned in the previous chapter that observations of strong point sources are the most sensitive way of judging the telescope performance. We present here some results obtained from the observations of strong point sources and their implications for the telescope performance. In the present context, "strong" refers to those sources which give a signal-to-noise ratio $\gg 5$ in each of the visibilities. As has been mentioned in Chapter **2,** the minimum detectable flux for GEETEE is ≈ 4 Jy. With a single row in the S array, this will be $\approx$ **40** Jy. Thus, any source stronger than **200** Jy will be a $> 5\sigma$ detection with a **single** row of the S array.

We analysed the following **5** sources as routine checks of the system **:** **36144** (Tau A), **36218** (Hydra A), **3C274** (Virgo **A)**, **36405** (Cygnus **A)** and **3C461** (Cas A). All these sources are unresolved as far as **GEETEE** is concerned, Their fluxes are approximately **2400** Jy, **1200** Jy, **4000** Jy, **24000** Jy and **40000** JY at **34.5** MHz. They cover a fairly wide range of R.A. and declination to give an overall picture of the telescope performance.

For the purposes of discussion, we would like to consider two sources, Cas **A** and Tau **A** and discuss the implications of their observations for the antenna performance :

<u>Amplitude distribution on the S arras</u>

If the correlation amplitude recorded in any given row n is An , then,

$$A_n \propto \frac{\sqrt{T_{EW}^{s}\, T_{n}^{s}}}{\sqrt{T_{EW}^{s} + T_{EW}^{b} + T_{EW}^{r}}\ \sqrt{T_{n}^{s} + T_{n}^{b} + T_{n}^{r}}} \qquad (3.1)$$

where T is the antenna temperature. The superscripts **s,b** and **r** refer to the contributions of the source, the background and the receiver respectively. The subscript n refers to the row number in the southern array. It is assumed here that the background is resolved out and is not contributing to the signal which is true in longer (> 3h) baselines. The visibility amplitude recorded in the 88 rows of the southern array at the time of transit of these two sources are given in Fig. **3.1** and Fig. **3.2** respectively. Fig **3.3** gives the ratio of these two sets of amplitudes, each set normalised to its average value. Figure **3.4** is similar to Fig. **3.3** but obtained from observing Tau **A** on two different days. Figure **3.5** is similar to Fig. **3.3** but for the source Cas **A** observed on two different days. The **r.m.s.** values of the scatter in the figures 3.1, **3.2, 3.3, 3.4** and **3.5** are 8 X, 5 %, 8 X, 2 % and 1.4 % respectively. This result and the anlysis done on other strong sources **imply** the following :

(a) the gains of the elements of the southern array repeat to an **r.m.s.** of 1 % as estimated from the same source on two different
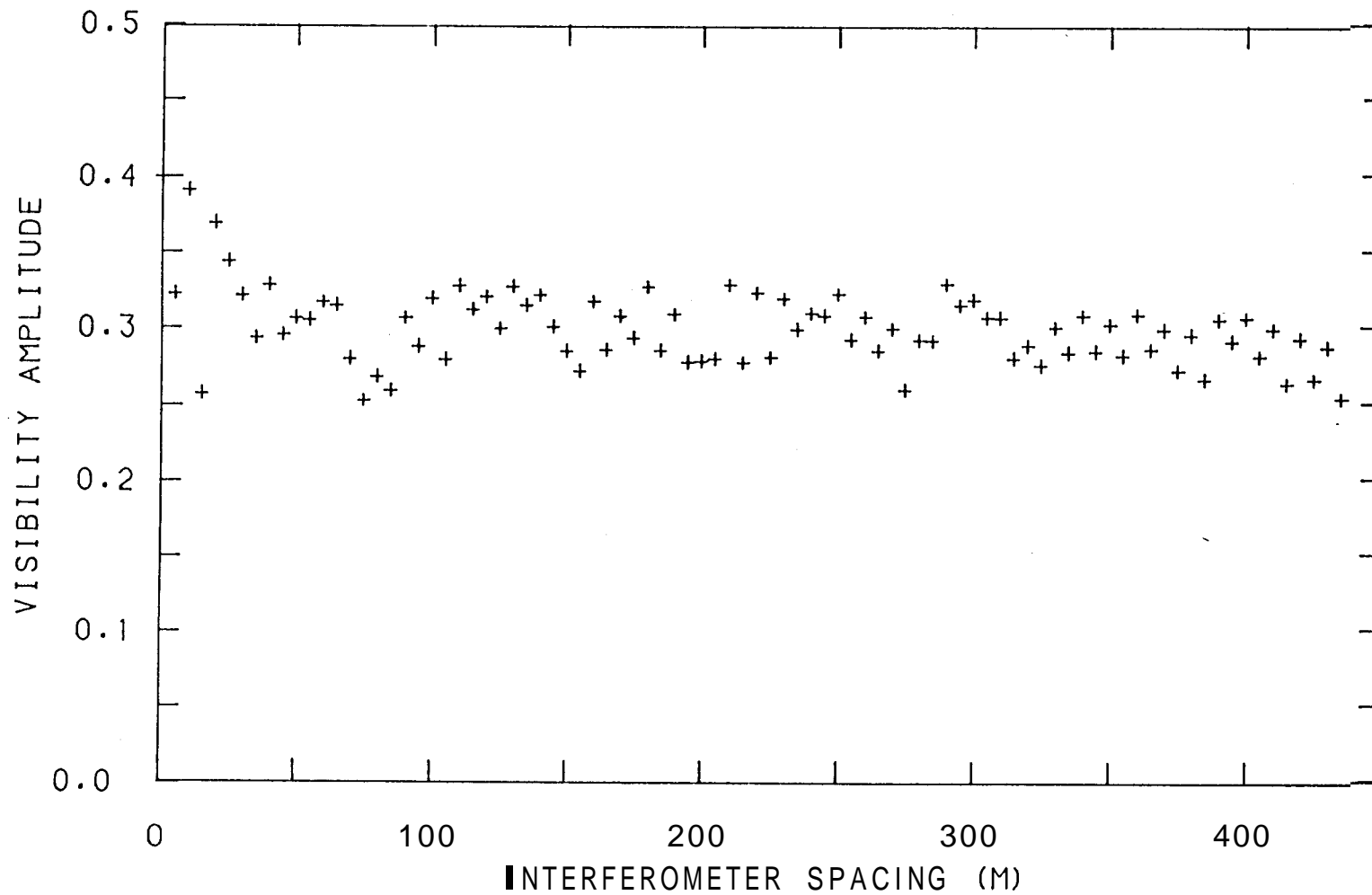
Fig. **3.1:** Amplitude of the visibilities recorded at the time of transit of Cas **A** as a function of the interferometer spacing in NS. The observed visibilities have been corrected for the band width decorrelation corresponding to the zenith angle of Cas A.
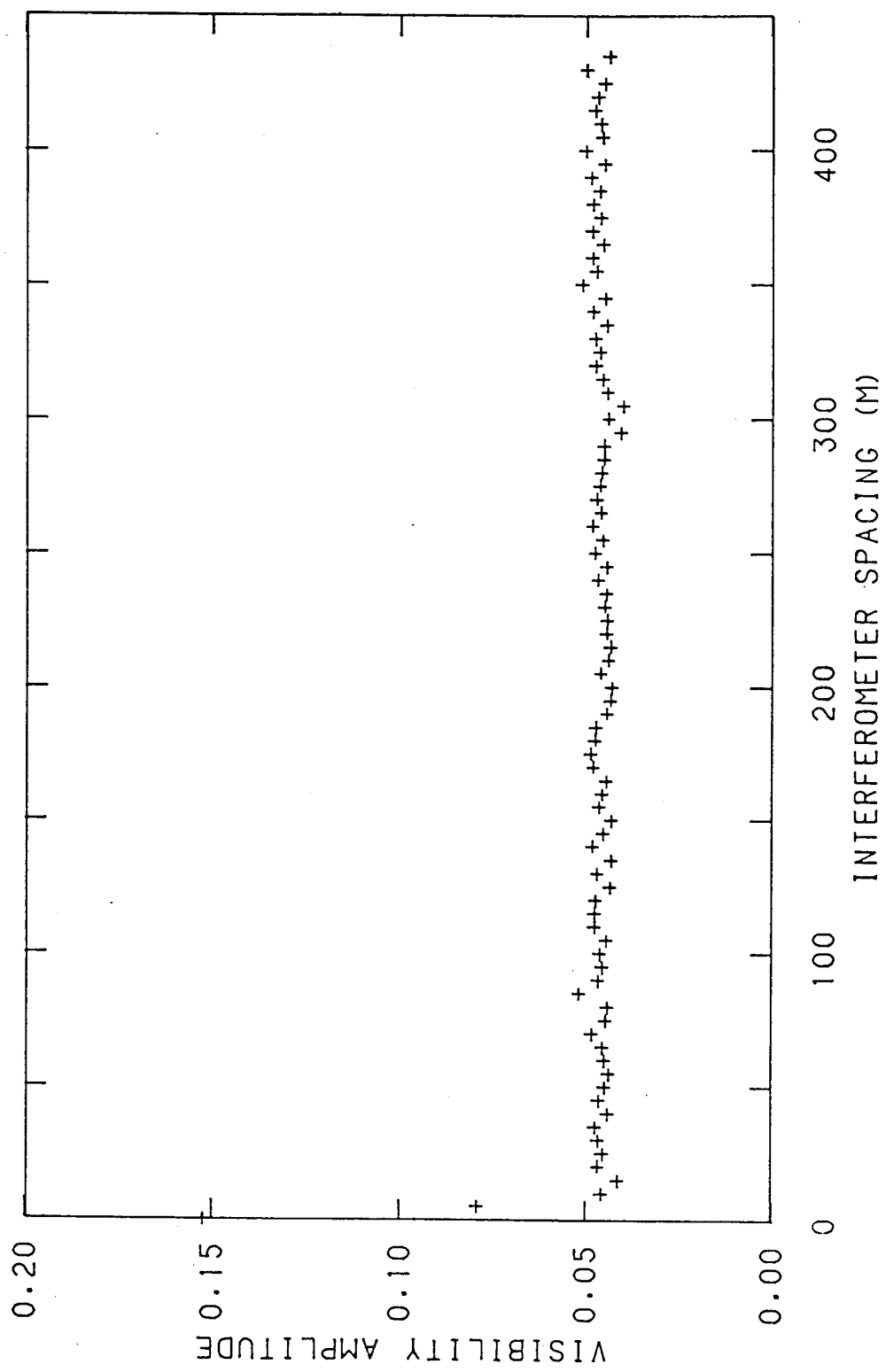
Fig. 3.2   Same as fig. 3.1 but for the source Tau A
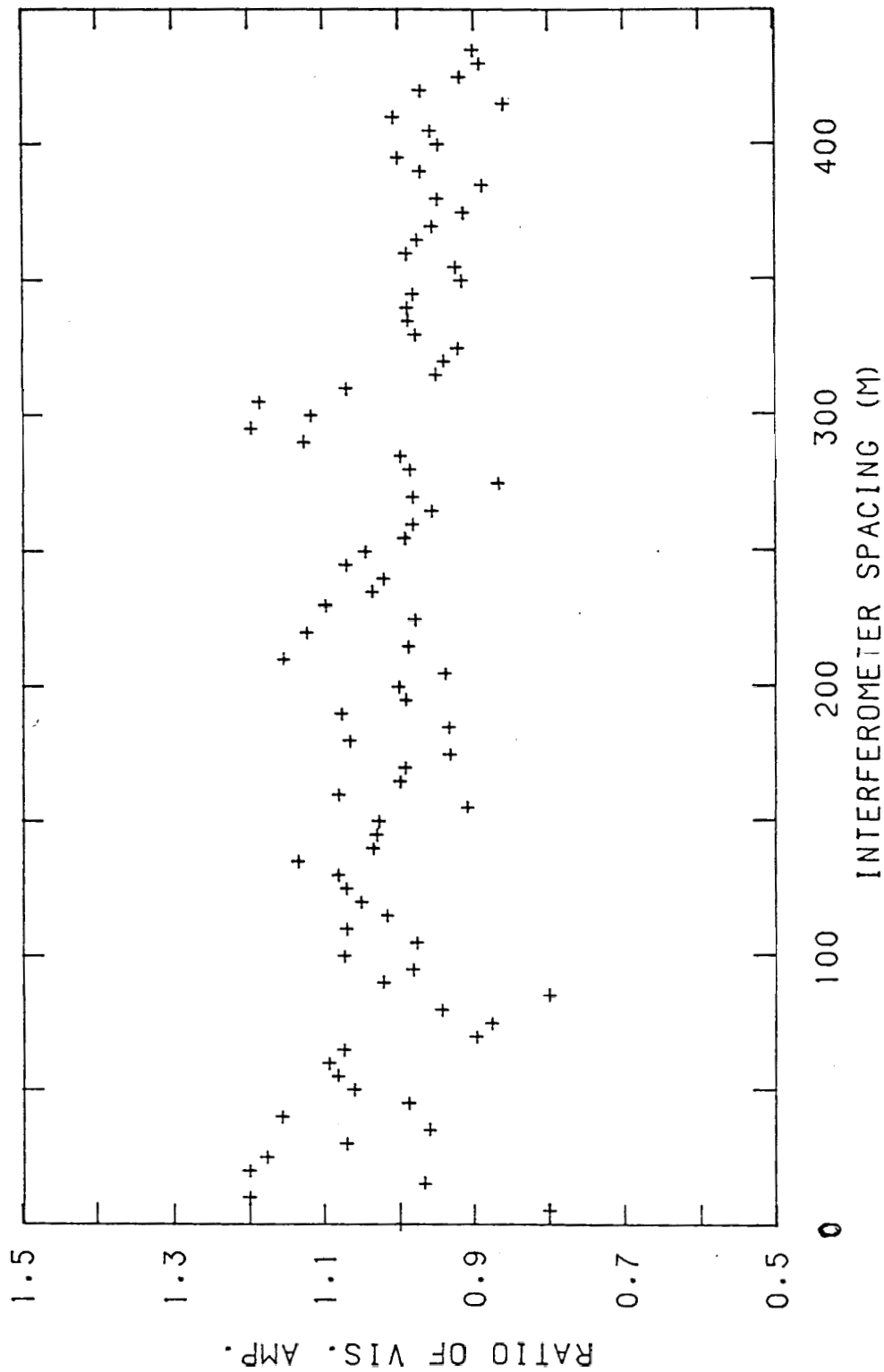
Ratio of amplitudes of visibilities as given by Cas A and Tau A. For any spacing n,

$$\text{ratio} = \frac{\left[\,N\,\sqrt{C_n^2 + S_n^2}\;/\;(\sqrt{C^2+S^2}\,)_{average}\,\right]_{Cas\,A}}{\left[\,\sqrt{C_n^2+S_n^2}\;/\;(\sqrt{C^2+S^2}\,)_{average}\,\right]_{Tau\,A}}$$

where average is over the interferometers 1 to 88.

Fig. 3.4: Same as fig. 3.3 but instead of Cas A, Tau A of another day is used Notice the reduced scatter as compared to fig. 3.3.

Fig. 3.5: Same as fig 3.3 but instead of Tau A, Cas A of another day is used.

days, and

(b) repeat to an **r.m.s.** of 6 X as estimated **from** 2 different sources (either on the same day or on different days).

Before we seek explanations for these two points **let** us look at the **r.m.s.** value of the scatter seen in the amplitudes o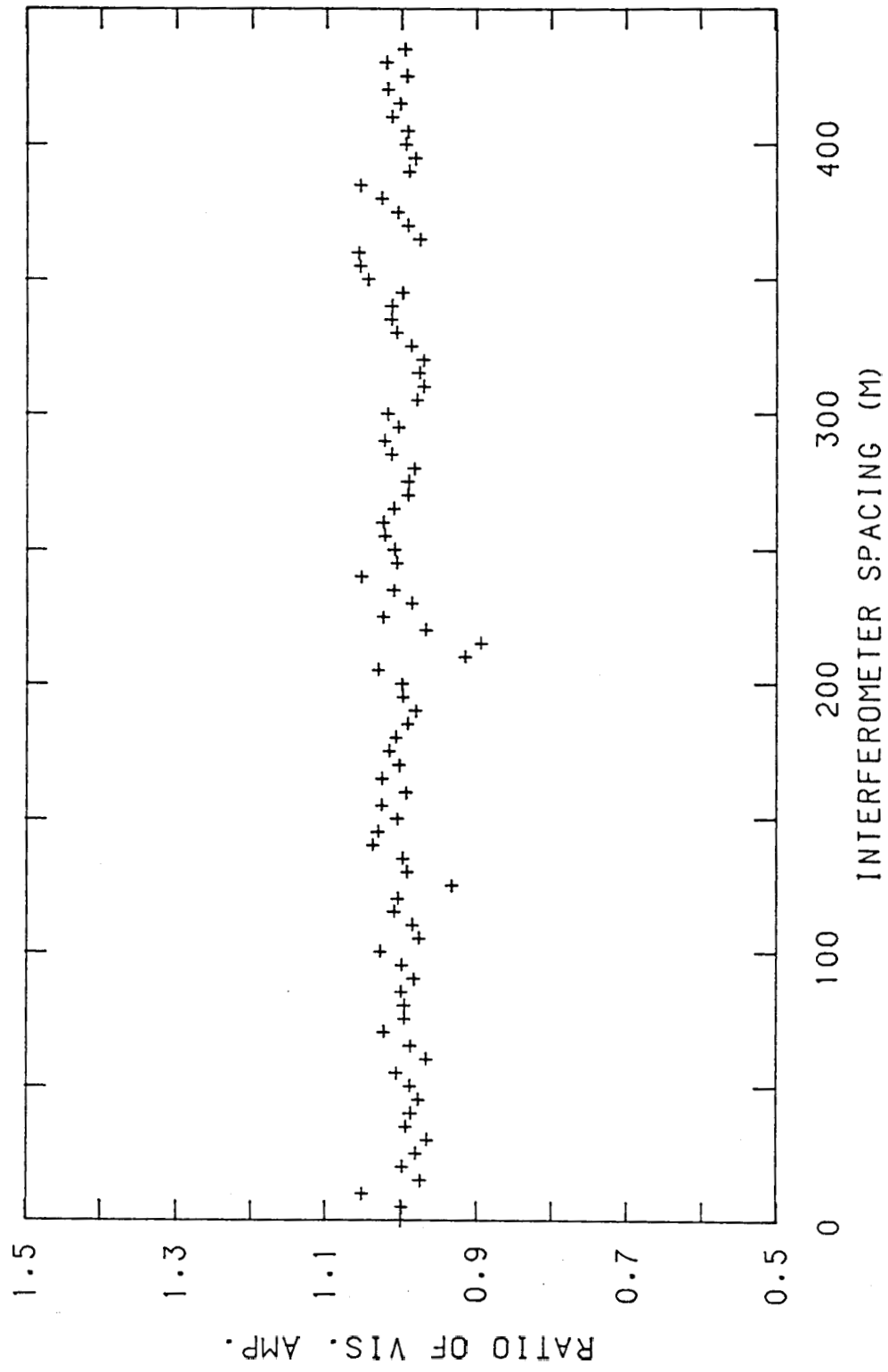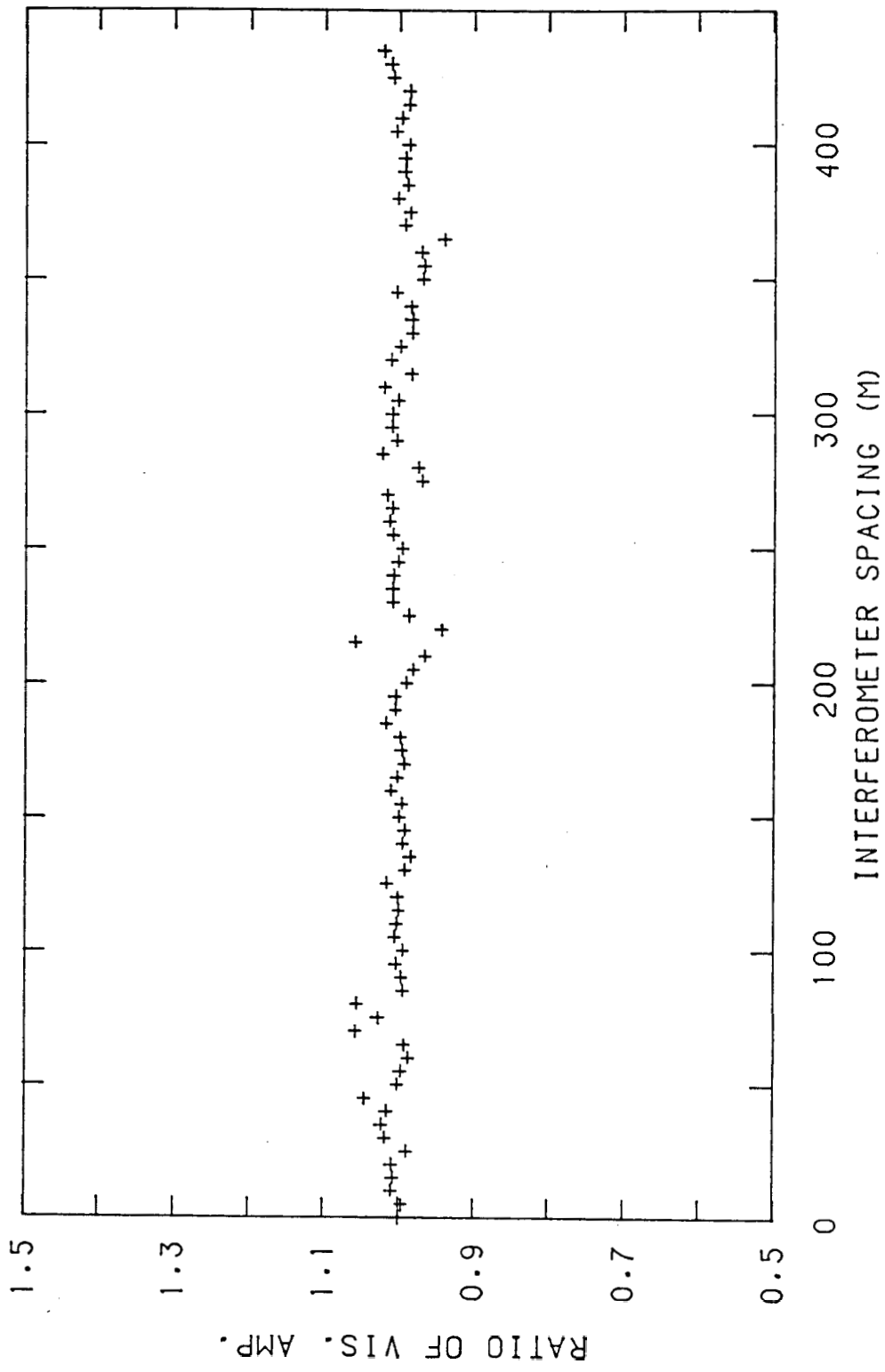f the visibilities recorded for a given source as seen for example in Fig. 3.2. An **r.m.s.** value of ≈ 5 % seen here could result from the following :

(1) variation among the 88 rows of the southern array of the loss before pre-amplification, and in the amplifier noise temperature, can account for ≈ 1 X **r.m.s.** (section 2.4.1 and eq. 3.1).

(2) an overall change of ≈ 0.5 dB in the gains of the basic units of the S array could lead to ≈ 12 % change in the T_n^S and consequently ≈ 6 % change in the A_n s measured at transit (eq.3.1). This appears to be an important possible cause for the scatter seen in Figures 3.1 and 3.2. Note that this change in gain affects T_n^b very little as T_n^b is the result of integrating the sky over the beam.

Result (a) can be understood as due to day to day variations in (1) and (2).

Result (b), however, implies a zenith angle dependent effect and is most likely due to the relative gains of the 88 units varying with the zenith angle.

<u>Instrumental **phase**</u> : Each of the 88 rows in the **S** array will have a phase difference **w.r.t** the EW array which is purely instrumental. This can be estimated using a strong point source and just as in the case of the amplitude of visibility of

the 88 baselines, it is important to know the variation of the instrumental phase as estimated from different sources, and also its variation with time.

If there is only one strong source in the sky at the time of observation then,

$$\phi_n = \tan^{-1}\left(\frac{S_n}{C_n}\right) = \frac{2\pi}{\lambda} d_n \sin\theta + \phi_{n,inst} \qquad (3.2)$$

Where,

S_n is the sine correlation recorded in the nth baseline,

C_n is the cosine correlation recorded in the nth baseline,

d_n is the distance of the nth baseline from the EW array,

θ is the zenith angle of the source, and

$\phi_{n,inst}$ is the instrumental phase to be estimated.

Figure 3.6 shows the difference in the instrumental phases as estimated from Cas **A** and Tau **A** as a function of the interferometer spacing. The linear part simply reflects the fact that there is a difference between the assumed and the apparent position of either one or both the sources. This is most likely due to refraction by ionospheric variations. The scatter on the other hand must reflect the system behaviour. The value of the **r.m.s.** fluctuation is 8°. Figure 3.7 is similar to Figure 3.6 but for the same source Tau **A** on two days. Figure 3.8 is similar to Figure 3.6 but for the same source Cas **A** on two days. From these three figures the following conclusions can be drawn :

(a) the instrumental phases repeat to an **r.m.s. of** $\approx 1^o$ from day to day as determined from the same source, and
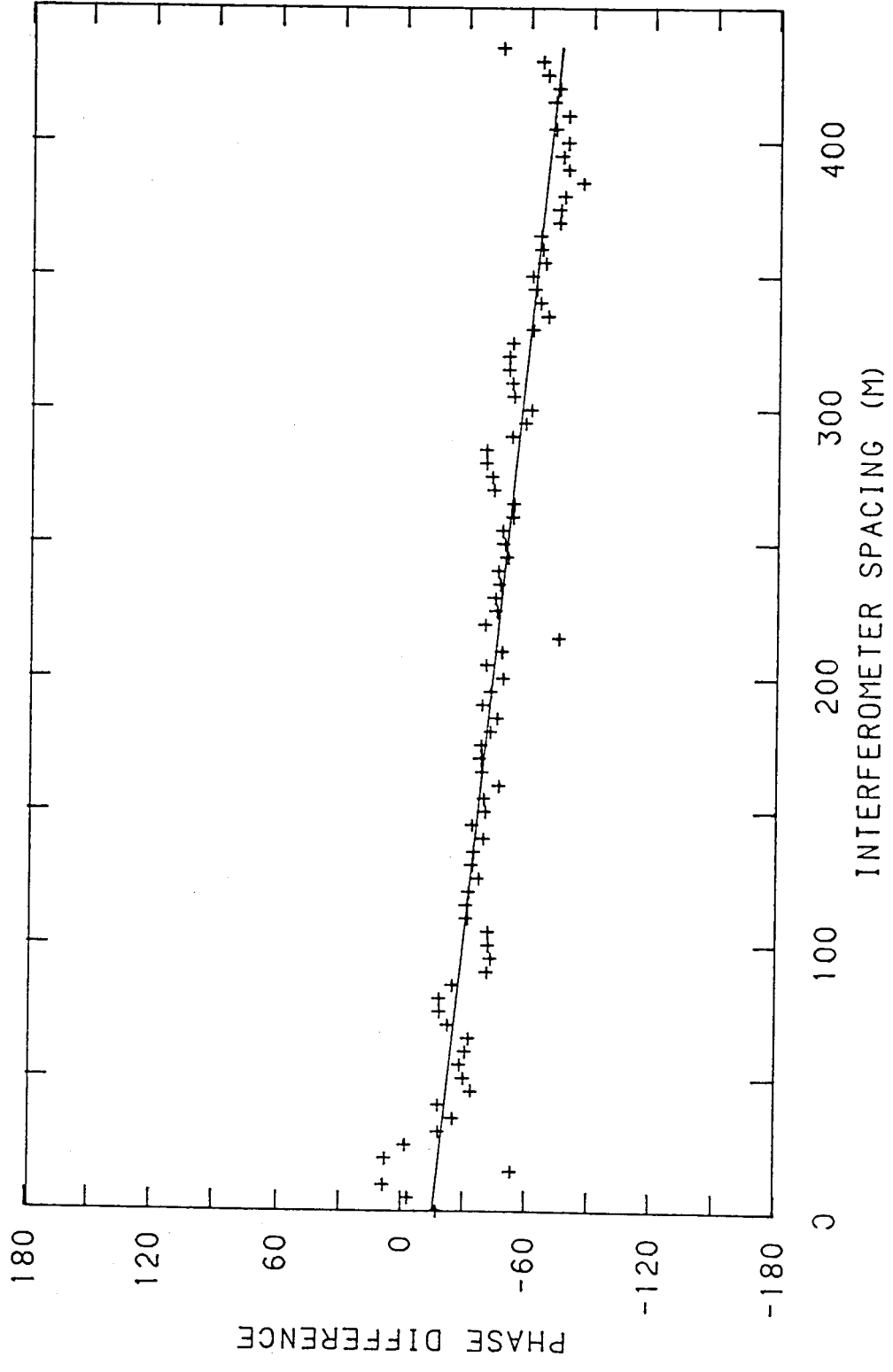
Fig. 3.6: Difference in the instrumental phase (in degrees) as a function of the interferometer spacing. The difference is obtained between the instrumental phases as given by Cas A and Tau A on the same day.
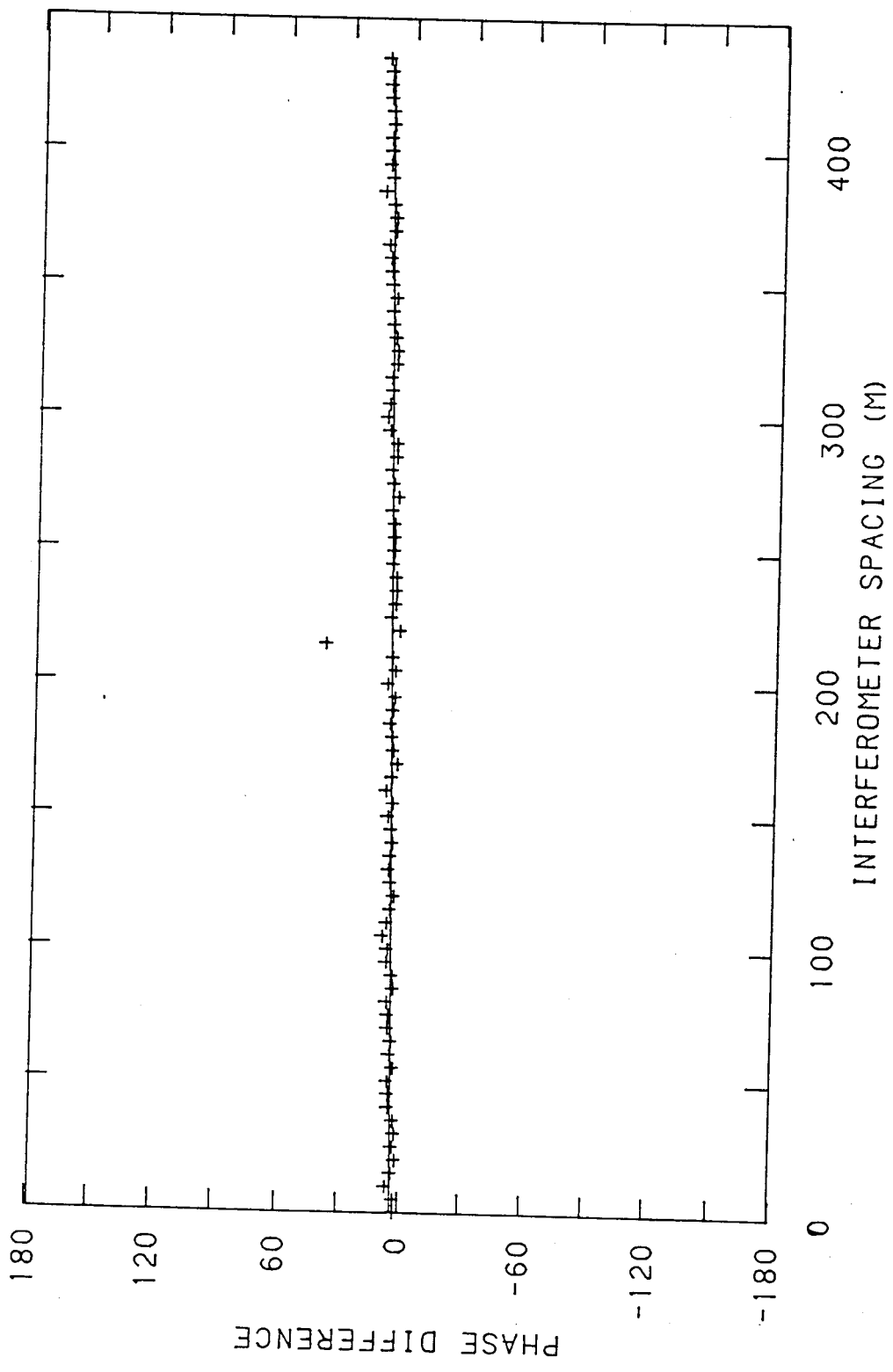
Fig. 3.7   Same as fig. 3.6 but instead of Cas A, Tau A of another day is used.   Notice the reduced scatter as compared to fig. 3.6.

PHASE DIFFERENCE

INTERFEROMETER SPACING (M)
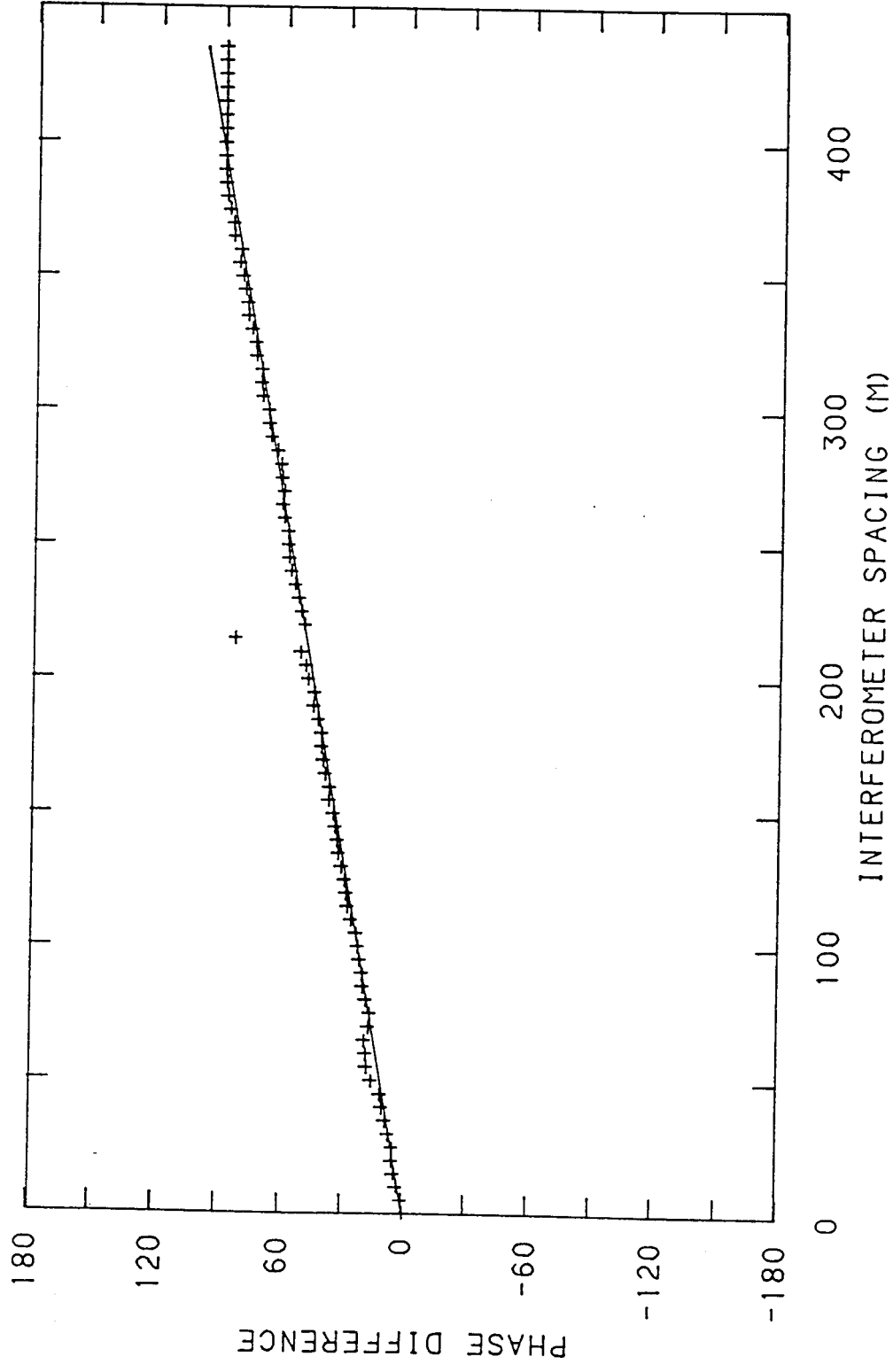
Fig. 3.8: Same as fig. 3.6 but instead of Tau A, Cas A of another day is used.

(b) to an **r.m.s.** of 6° from source to **source** (either on the same day or on different days)

These conclusions are similar to those drawn about the gains of the elements. In all possibility, the causes are similar too.

As will be discussed later in this chapter, the scatter in the amplitude and phase ditribution from one point source to another results in undesirable residual sidelobes even after CLEANing.

<u>The EW antenna</u>: Figures **3.9** and **3.10** show the **amplitude** and phase distribution on the EW aperture as given by fourier transforming the beam given by Cygnus **A**. The amplitude and phase distribution show a scatter over the aperture with an **r.m.s.** of **1** dB and 10° respectively. The **EW** beaa corresponding to this is shown in figure **3.11**. To get an idea of the stability of this illumination pattern, we show in figures **3.12** and **3.13** the difference between the **EW** beams of Cyg **A** on two different days (each normalised to its peak value) and the difference between the EW beams of Cyg A and Tau A (each **normalised** to its peak value) on the same day. They both show scatter with an **r.m.s. of** $\approx$ **2%**. Thus, the **EW** beam repeats to an accuracy of **2%** of its peak value. This is an upper limit to the variation in the EW beam pattern since the scatter includes any error due to the misalignment of the two beams while subtracting owing to the finite sampling time and also due to any amplitude scintillation which may offset the normalisation.
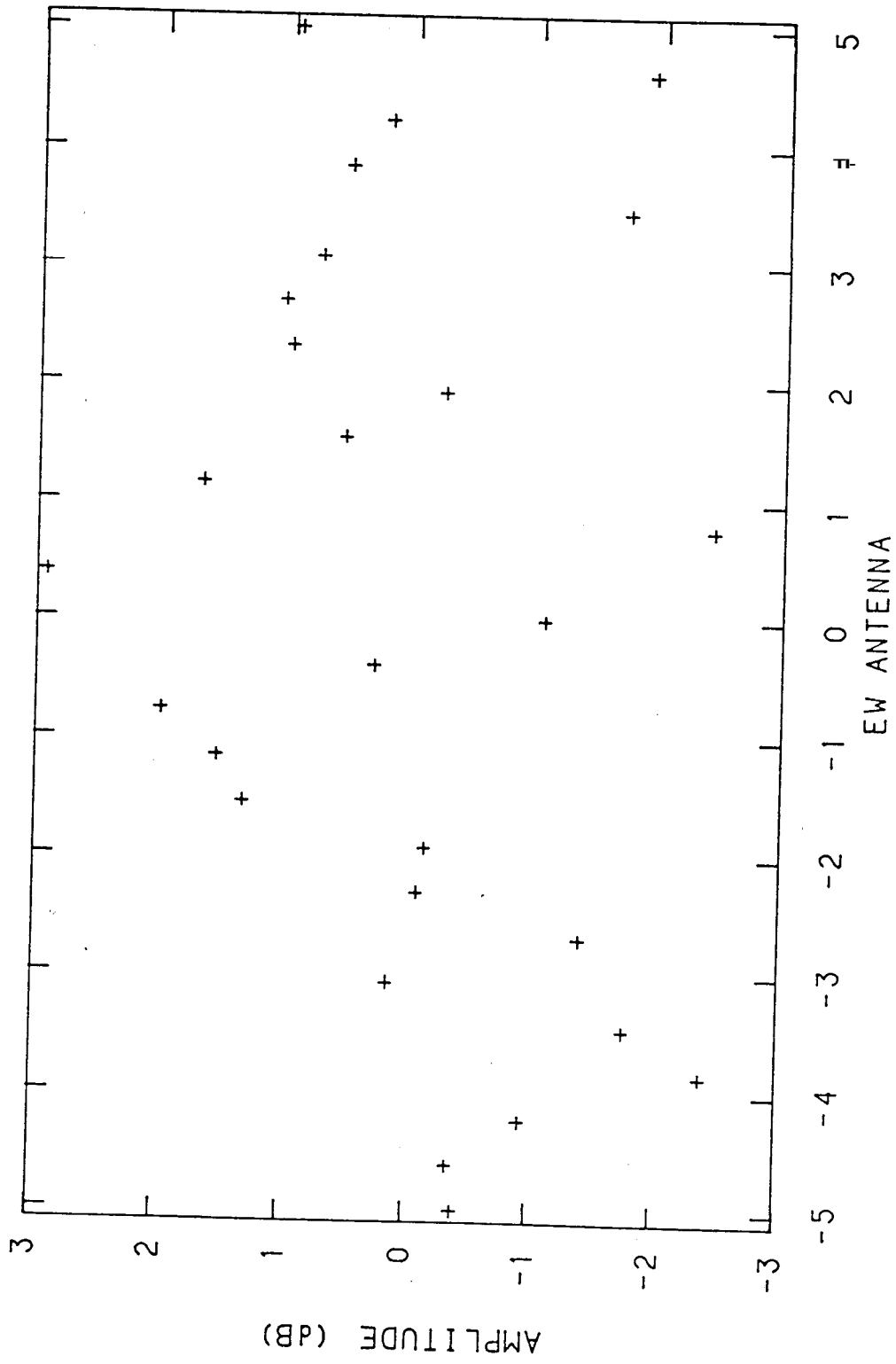
Fig. 3.9: Amplitude distribution across the EW aperture as obtained by fourier transforming the EW beam given by Cygnus A. Length of the X axis (-5 to +5) is equal to the length of the EW aperture. Zero corresponds to the centre of the EW antenna.
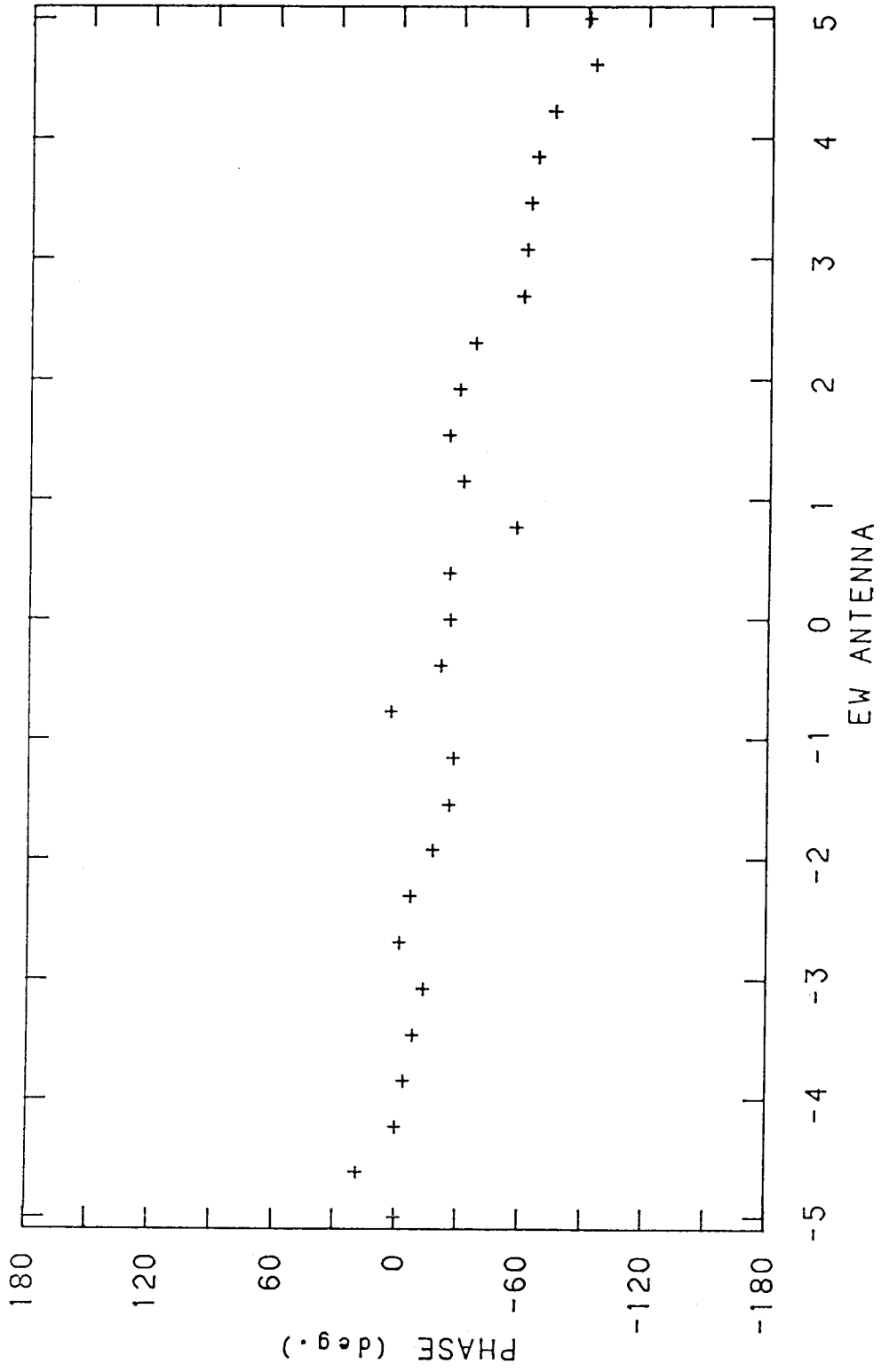
Fig. 3.10: Phase distribution across the EW aperture
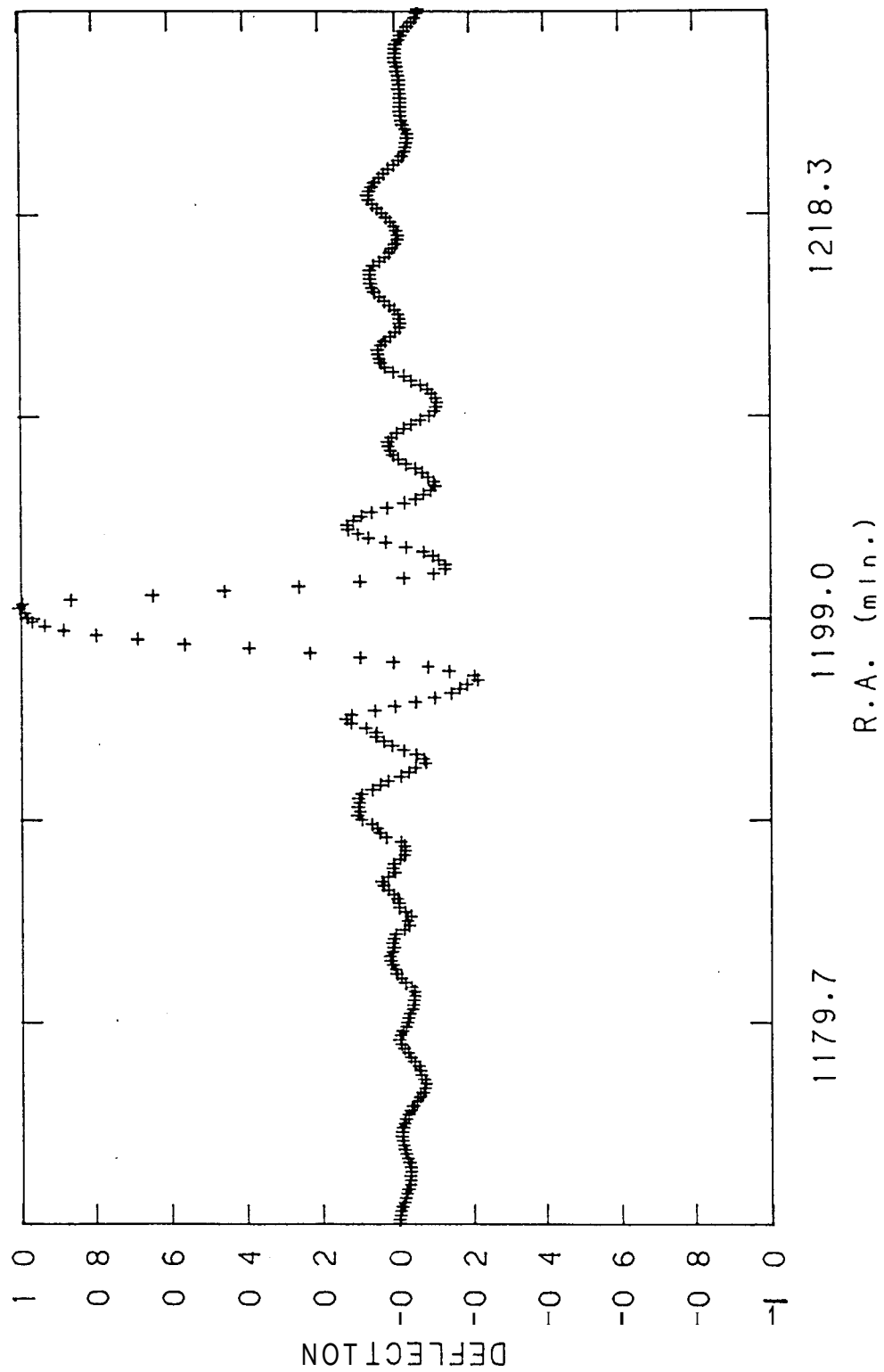
Fig. 3.11: WW beam pattern as given by Cygnus A corresponding to the illumination pattern given in figs. 3.9 and 3.10.
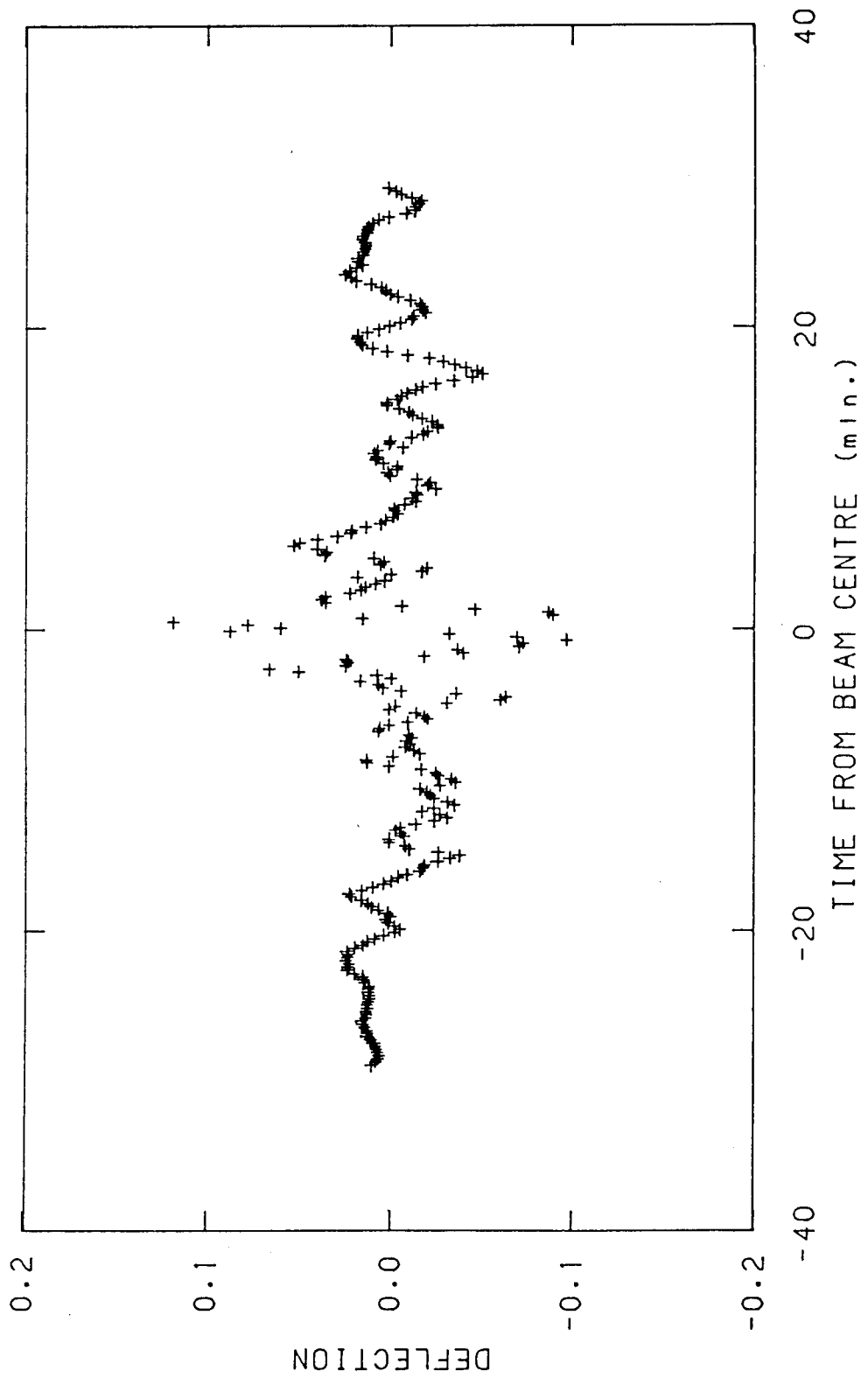
Fig. 3.12 Difference in the EW beams of Cygnus A on two different days
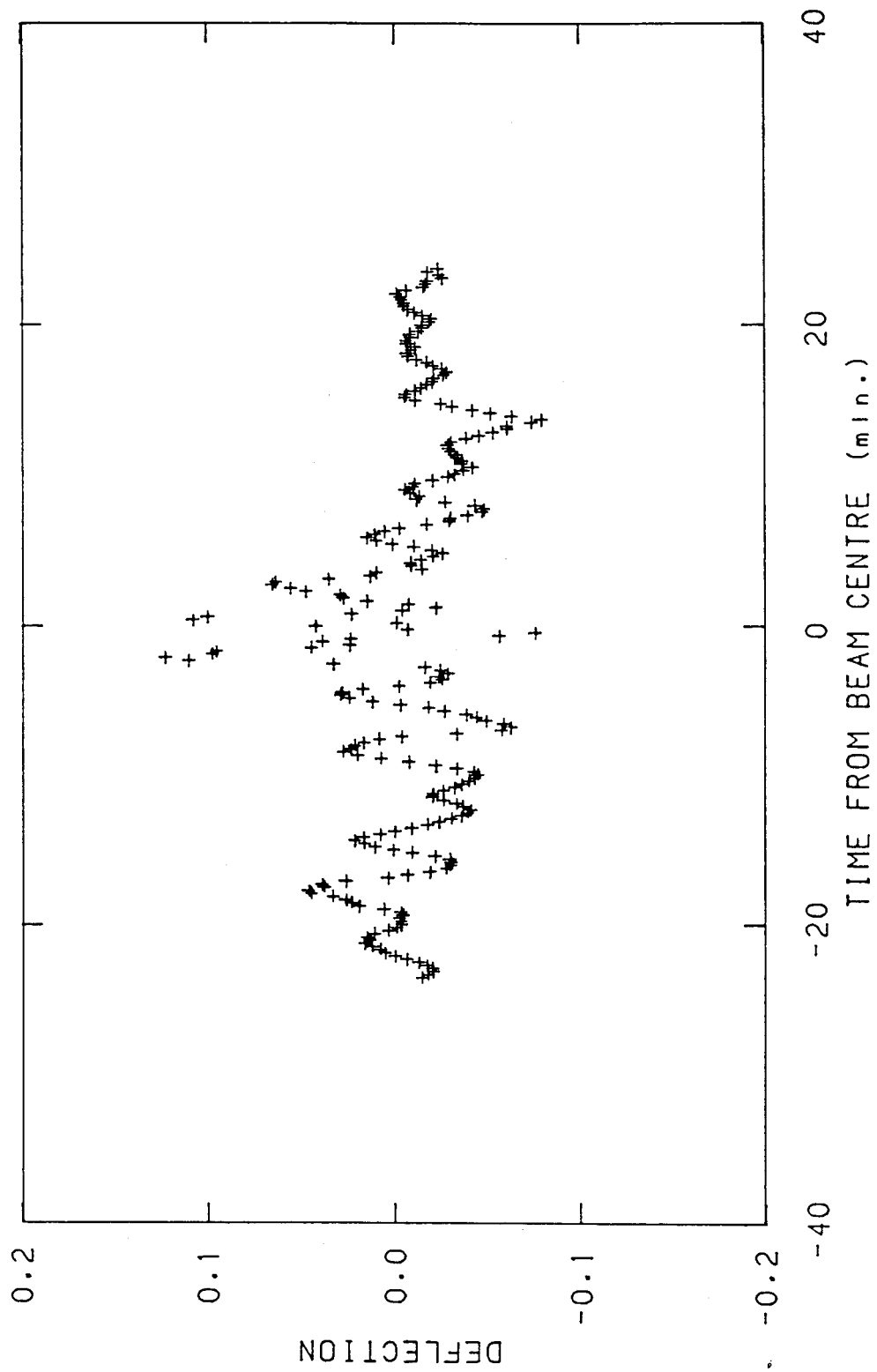
Fig. 3.13: Difference in the EW beams of Cygnus A and Tau A: There is no significant difference in the r.m.s. value of the scatter in this figure and in fig. 3.12.

3.2 DATA ANALYSIS

3.2.1 Producing the raw map

The brightness distribution $B(l,m)$ in the sky is related to the visibility $V(u,v)$ through the fourier transform **relation as** follows :

$$B(l,m) = \iint V(u,v)\, e^{-j2\pi(ul+vm)}\, du\, dv \qquad (3.3)$$

and the raw map or the dirty map $B'(l_0,m_0)$ at any position l_0, m_0 in the sky is the convolution of the brightness distribuiton with the antenna response $P(l,m)$:

$$B'(l_0,m_0) = \iint P(l-l_0, m-m_0)\, B(l,m)\, d\Omega \qquad (3.4)$$

(Christiansen and Hogbom 1985).

In the present case, the recorded visibilities are fourier transformed along the north-south direction to produce a strip of dirty map at each instant of time.   Hermitian symmetry in the recorded visibilities is assumed (recall the discussion about 'T' and '+' arrays in Chapter 2).   The fourier transform naturally produces the raw maps in the q (=sin(**zenith** angle)) coordinate.

The procedure for obtaining a raw or dirty map is indicated in Table 3.1.   Some additional comments about Table 3.1 are as follows :

(a) The   total   power   from   the EW array and   from   one representative   element   in the S array are recorded continuously.

Table 3.1   A flow chart of the procedure used to obtain the raw maps

```
                          ┌─────────────────────────┐
                          │128 channels of recorded │
          ┌───────────────│data, pre-integration of │───────────────┐
          │               │262 ms                   │               │
          │               └─────────────────────────┘               │
          ▼                            ▼                             ▼
┌──────────────────┐       ┌──────────────────────┐     ┌──────────────────────┐
│ 88 complex       │       │Noise calibration at  │     │Threshold detector +  │
│ visibilities     │       │the end of the hour,  │     │sampler + correlator  │
└──────────────────┘       │$\mathcal{S}_{cal}$   │     │output, $\mathcal{S}_S$│
          │                └──────────────────────┘     └──────────────────────┘
          ▼                            ▼                             ▼
┌──────────────────┐       ┌──────────────────────┐     ┌──────────────────────┐
│24 s integration  │       │24 s integration      │     │24 s integration and  │
│and 12 s interlaced│      └──────────────────────┘     │12 s interlaced       │
│sampling          │                   │                │sampling              │
└──────────────────┘                   ▼                └──────────────────────┘
          │            ┌──────────────────────────────┐              │
          ▼            │$\mathcal{S}_{cal}=\frac{2}{\sqrt{\pi}}\int_0^{x_{cal}}e^{-t^2}dt$ │  ┌─────────────────────────┐
┌──────────────────┐   │                              │  │$\mathcal{S}_S=\frac{2}{\sqrt{\pi}}\int_0^{x_S}e^{-t^2}dt$│
│Subtract correlator│  │$x_{cal}=\frac{V_{th}}{\sqrt{2}\,\sigma_{cal}}$│  │$x_S=\frac{V_{th}}{\sqrt{2}\,\sigma_S}$│
│offsets           │   └──────────────────────────────┘  └─────────────────────────┘
└──────────────────┘
          │                                                          │
          ▼                                                          ▼
┌──────────────────┐                                     ┌──────────────────────┐
│Apply van-Vleck   │                                     │                      │
│correction to     │─────────────────────────────────────│$\sigma=\frac{x_{cal}}{x_S}$│
│correct for       │                                     │                      │
│one-bitting and   │                                     └──────────────────────┘
│obtain $\mathcal{S}_c'$│
└──────────────────┘
          │
          ▼
┌──────────────────┐
│Correct for the   │
│instrumental phase│
│and obtain $\mathcal{S}_c$│
└──────────────────┘
          │
          ▼
┌──────────────────┐
│De-normalise the  │
│correlation       │
│coefficients      │
│$\mathcal{S}=\sigma_{EW}\sigma_{NS}\mathcal{S}_c$│
└──────────────────┘
          │
          ▼
┌──────────────────┐     ┌──────────────────┐     ┌──────────────────┐
│Fourier transform(1d)│  │Carry out the above│    │Raw map of 1 hour │
│to obtain a strip of │─▶│procedure for all  │──▶ │by entire NS      │
│raw map covering the │  │samples in an hour │    │results           │
│complete sky in NS   │  └──────────────────┘     └──────────────────┘
└──────────────────┘
```

(b) The error function integral is evaluated using its analytical approximation as given in the Handbook of Mathematical Functions by Abramowitz and **Stegun.**

(c) As long as the threshold value, V_{th}, remains constant it is not necessary to know its value to estimate the power. Since the calibration noise power also goes through the same threshold, V_{th} can be eliminated by taking the ratio of $\frac{x_{cal}}{x_s}$.

(d) The **88** complex visibilities are not recorded continuously in the sense that there is time multiplexing between a group of **4** rows of the S array. Thus, the **24 sec** integration time refers to the total stretch of data that is integrated. The effective integration time is 6 **sec.**

(e) Assuming Hermitian symmetry a **1024** point one-dimensional FFT is performed on each set (resulting from an integration of 24 **sec)** of **88** complex visibilities to obtain a strip of raw map that stretches over the entire sky in the NS direction. Successive strips are obtained by the successive sets. Raw maps are produced in sizes of 1 Hr **x** entire NS. The **1024** points are uniformly placed in **sin(zenith** angle) coordinate. Thus the raw maps are produced in a time and **sin(zenith** angle) system. Since the successive baselines are separated by **5** m, the **FFT** produces maps in the range of **-0.869** to **+0.869** in the **sin(zenith** angle) coordinate system. If, in the above procedure, only the measured **88** complex visibilities are used then the output of the FFT will be complex. This can be called a **'complex map'.**

(f) Similarly, raw maps are produced for all the 24 hours of right ascension.

3.2.2 Interference on the raw map

Interference which is of short duration in time is easily detected on the raw map by its appearance. There were only about half a dozen places where such spikes could be seen. Each of these spikes had corrupted the data for < 30 **sec** in **time** (it may be recalled that the resolution of the EW antenna along RA is 84 **sec** of time at 0° dec.). An 8th order polynomial fit to the adjacent data stretches was used to fill in these gaps. This fit works very well as was verified by trying it on data stretches where there is no interference.

3.2.3 **CLEANing** the dirty map

The   dirty map is the convolution of the brightness distribution in the sky with the antenna response **(eq.(3.4))**. To obtain the brightness distribution in the sky the dirty map has to be deconvolved. There are many methods of deconvolution. We discuss here some of them and the problems in adopting them in the present case:

Convolution along RA and dec: Given the dirty beam in RA it is possible to come up with a 'correcting' beam in RA which when convolved with the dirty beam reduces the **sidelobe** levels in RA to $\approx 3\%$ (on the lines given in Christiansen and Hogbom 1985, p. 85). Similar convolution can be tried along declination also. For this method to work, it is important to know the resolution of the dirty beam. Given dirty maps of large angular extent in

time and **sin(zenith** angle) system, this method poses a problem. The dirty beam is invariant along **NS** since the dirty maps are in **sin(zenith** angle) coordinate system and the desired convolution can be performed. However, convolution along **RA** is not straightforward - consider a source **A** at a declination δ_1. Its sidelobes in **RA** at different declinations will have their widths $\propto \sec(\delta_1)$. To remove the **RA** sidelobes of **A** at a different declination, say, δ_2 the correcting beam will still have to correspond to the declination δ_1. This, however, will be inappropriate for some other source B which is at the declination δ_2. This problem can be solved by going to spherical coordinates but involves large data handling capability, interpolation of the data, etc. which is not a desirable scheme.

Two **1-D CLEAN**: Given the dirty beams along **RA** and dec., it is in general possible to adopt **CLEAN** (Hogbom 1974) or its variant (as discussed further in this section) to deconvolve the dirty maps. In this case, however, this procedure cannot be adopted due to the complex nature of the EW beam, unless, of course, **CLEAN** is performed with the complex dirty beams (along **RA** and dec) on the complex dirty map. This was not pursued further due to its 'complex' nature.

This brings us to the next possibility and that is of using the two dimensional point spread function (PSF) or the two dimensional response of the antenna. Given the PSF and the dirty map, deconvolution can be attempted. We discuss below several problems in obtaining the **PSF** and in adopting the conventional **CLEAN.**

3.2.3.1 How to obtain the Point Spread Function ?

The PSF that we need is the antenna response to a point source in the sky. The dirty map around a point source will be the PSF if the source is extremely strong and there exists a sufficiently wide field around the source which can be considered relatively empty. At low frequencies, due to the ubiquitious galactic background this situation is hardly true. Though sources like Cas A and Cyg **A** can be considered very strong from the point of view of the noise in the map, the criterion of empty field around them is hardly met. So, the PSF has to be generated.

<u>Complex nature of the antenna **response**</u>: Since the telescope is used in the correlation mode (**i.e.** EW **x** S) and the two arrays are expected to be uniformly illuminated, it is tempting to suggest that the PSF is simply the product of two sinc functions one along the EW direction and the other in the NS direction. However, this does not give us the PSF for two reasons:

1) the **EW** beam departs from the sinc function significantly.

2) the **EW** beam is complex since its illumination pattern is not Hermitian symmetric (see Fig. **3.9** and Fig. **3.10).**

Given these problems, one may generate the point spread function by obtaining cuts along RA and dec. at the source position in the complex dirty map of a strong source and multiplying them. This might be a reasonable approach since in the correlation **mode** one produces the 2D response by multiplying the response of the individual telescopes.

Generating the PSF: The antenna response, b, to a point source at (l_o, m) can be written as

$$b\left(l-l_o, m-m_o\right) = b_{EW}\left(l-l_o, m-m_o\right) b_{NS}\left(l-l_o, m-m_o\right) \qquad (3.5)$$

where b_{EW} and b_{NS} refer to the far-field voltage radiation patterns of the EW and the S arrays respectively. Since the EW and the S arrays have slowly varying patterns along NS and EW respectively, this can be approximated to

$$b\left(l-l_o, m-m_o\right) \simeq b_{EW}\left(l-l_o, m_o\right) b_{NS}\left(l_o, m-m_o\right) \qquad (3.6)$$

Both b_{EW} and b_{NS} are in general complex and

$$b_{NS}\left(l_o, m-m_o\right) = \frac{1}{2} C_1 + \sum_{n=2}^{88} \left(C_n + j S_n\right) e^{j\phi_n} \qquad (3.7)$$

where,

$\quad$ C_n and S_n are the cosine and sine correlations recorded in the $\mathbf{n^{th}}$ unit of the **S** array.

$\quad$ $\phi_n = 2\pi(n-1)d(\sin(\theta)-\sin(\theta_o))/\lambda$

$\quad$ m : $\sin(\theta)$

$\quad$ $\mathbf{m_o}$ = $\sin(\theta_o)$.

The dirty map at any instant of time is a summation of eq. (3.7) and its complex conjugate and hence is equal to the real part of eq. (3.6). Hence the **PSF** is generated by obtaining the complex cuts along RA and dec. of the point source response and obtaining the real part of the product.

Producing the **PSF** in **practice**: There are several points to be borne in mind in constructing the **PSF** according to the above recipe:

1) Which source should be used to produce the PSF ? - Ideally one should use a strong source at zenith in an empty background. In such a case the response of the source will reflect any **north-south** asymmetries in the antenna behaviour.   The closest one could come to meeting this requirement was Cygnus A (≈ 25000 Jy and at a zenith angles 26°).   A complex map was produced around Cyg **A** and the complex response in RA and dec was obtained.

2) To what extent can one attempt to construct the PSF ? - The basic criterion here is that the expected antenna response of the source should be well above the noise on the map.   Along the declination this is true over the full length of the map and this gives a natural size for the PSF along NS and that is the full extent of the map from -0.86 to 0.86 in **sin(zenith** angle) coordinates. Along RA, the sidelobes of Cyg A can be seen for **+3** hour around transit.   However, beyond $\approx$ **+1** hour in RA the curvature of the sidelobes becomes significant (see Appendix **1)** and there is no point in going beyond this extent. This problem can be overcome by transforming to spherical coordinates. But this will involve interpolation of the data and enormous amount of data handling and we have not attempted to do this in this thesis.   Instead, the length of the complex beam along RA **was** restricted to minimise this effect. Therefore the derived PSF is **+1** hour in RA and has the full extent in declination.   The curtailed size of the PSF along RA will, of course, affect the dynamic range of the map.

3) The galactic background also contributes to the complex beam. One can get a feeling for which baselines are sensitive to the

background by looking at the visibility amplitudes as a function
of baseline when there is no strong source in the EW beam. This
exercise revealed a monotonic decrease in the visibility
amplitude from the Ist baseline to the 7th baseline. The
contribution of the background was indistinguishable from the
noise in the remaining long-baseline S array elements. So, the
sky background contribution is predominantly present in the first
seven rows of the S array. To minimise the effects of the
background in the generation of the PSF, the measured
visibilities in the first seven baselines were replaced by
effective values. These were calculated by taking the amplitudes
to be the average amplitude of the 8 to 88 th baselines (Since
all the rows of the S array are similar, this procedure is a
reasonable one). In other words, the recorded visibilities in 1
to 7 are replaced by:

$$(C_n , S_n) = \langle A \rangle (\cos \phi_n , \sin \phi_n), \quad n = 1 \text{ to } 7 \qquad (3.8)$$

where, $\langle A \rangle$ is the average of the amplitudes of the visibilities
in the baselines 8 to 88 and $_n$ is the progressive phase
gradient. This modification was incorporated while generating the
complex maps around Cyg A for the purpose of obtaining the
complex beams.

4) The effect of ionospheric scintillation - If the complex map
generated is affected by scintillations then it will affect the
derived PSF. To minimise the effects of scintillation, the
complex beam along RA has been convolved with a .sinc function

beam corresponding to the EW antenna size. This smooths out any amplitude scintillations over time scales shorter than the time (at 0° dec.) corresponding to the EW resolution.

5) Effect of bandwidth decorrelation (BWD) -Bandwidth decorrelation refers to the loss of correlation between signals with finite bandwidth due to a finite delay between them. A delay of A t between the signals of rectangular bandwidth leads to a decorrelation D given by:

$$D = \frac{\sin(\pi \Delta \nu \Delta t)}{(\pi \Delta \nu \Delta t)} \qquad (3.9)$$

In the present case, Δt = (n-1)dsin(θ)/300 is the delay in μs. Here, n is the S array row number from 1 to 88, d is the spacing between the rows (= 5 m), and θ is the zenith angle. The bandwidth of our observation is 200 KHz. While generating the complex map around Cyg A the correlations have been corrected for the BWD.

6) Other sources present along the complex beam: The implicit assumption in generating the PSF by the multiplication of the complex beams along RA and dec is that no other sources are present along the cuts. However, we do not think that this is a serious problem when one is using a strong source like Cygnus A.

7) Interference will also affect the complex beams. An examination of the complex map around Cygnus A showed that interference was not a serious problem.

3.2.3.2 CLEAN

In the conventional method of **CLEANing** the maps (Hogbom 1974) one proceeds by locating successive maxima in the dirty map

and at each stage subtracting the dirty beam placed at the location of the maximum. The height of the dirty beam is usually chosen to be a fraction of the maximum (≈ 0.2, called loop gain) for subtraction each time. Each time a maximum is located, a delta function whose height is the same fraction of the maximum as is chosen for the beam subtraction, is placed at the position of the maximum in a separate 'CLEAN map'. This process is repeated until a pre-determined level in the dirty map is reached (usually ≈ 5 times the **r.m.s.** value of noise). At the end, the CLEAN components are convolved with a 'good' beam, usually a Gaussian of full-width-half-maximum the same as that of the dirty beam. The residues in the dirty map are then added. The implicit assumption in this method is that the sky is empty except for the point sources. In addition, the **'emptyness'** is also a function of the dirty beam. In the present case, the dirty map contains point sources as well as the background. In addition, the background varies over the region being **CLEANed.** This poses problems if one uses CLEAN in its original form. Consider a case like the one shown in Figure 3.14 where two sources **A** and B are on a background. The source A has a height of A_{max} above zero while its height above the local background is only A'_{max}. Conventional CLEAN will pick up A and proceed. It may be seen, however, that the sidelobes present in the map do not correspond to this but to A'. In order not to oversubtract the source response, one could use a very small loop gain and avoid the danger. This, however, slows down the whole process considerably. In addition, if the background is **varying** over the
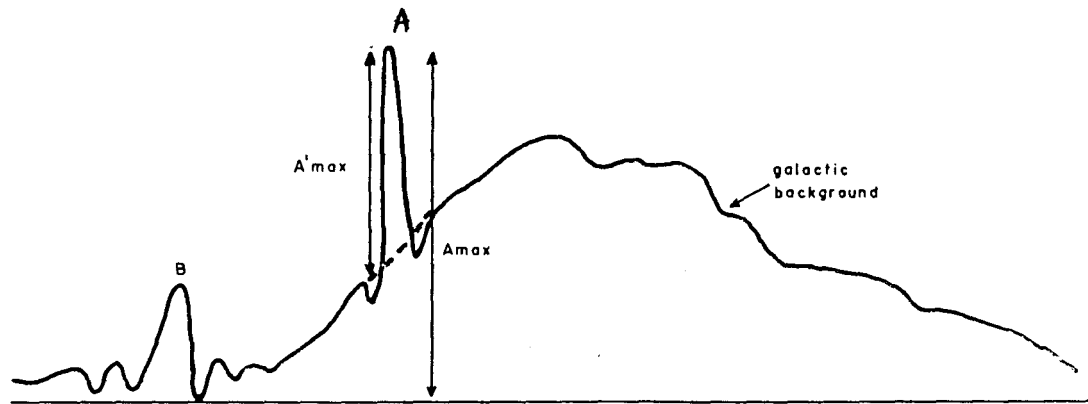
Fig. 3.14: Problems in CLEANing maps which contain both point sources and a varying background. The sidelobe level, in the map due to the source **A** corresponds to a height of A_{max} and not to A_{max}. It will take a considerable time before sources like B can be picked up for CLEANing.

region being CLEANed, it will take a much longer time before CLEAN can deconvolve the maps to responses from sources like B (Fig. 3.14) - in the mean time the algorithm would have picked up the variations in the background as maxima and carried out the process of CLEAN. This is not a desirable situation at all.

There have been earlier attempts to take care of large scale structures while CLEANing. Wakker and Schwarz (1988) for example have proposed Multi Resolution CLEAN (MRC). In this algorithm the dirty map is smoothed to a lower resolution and subtracted from the original dirty map. So one has a 'smooth map' and a 'difference map'. The dirty beams corresponding to these two maps are also generated and the CLEAN applied on both the maps.
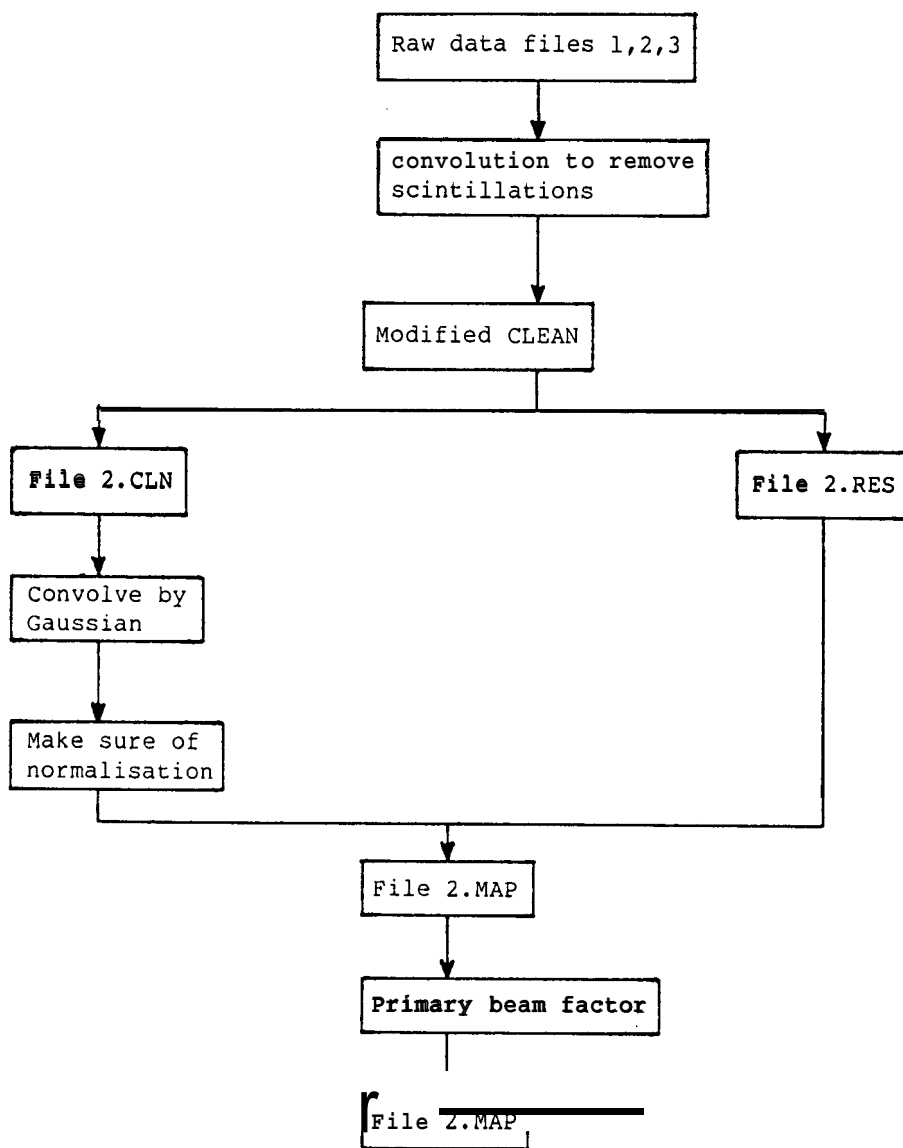
Modified CLEAN :

We have adopted the 'local maximum criterion' instead of the 'global maximum criterion' adopted in both CLEAN and MRC CLEAN. Instead of locating the maxima in the dirty map, we locate the maxima in the difference, where the difference at any given point in the dirty map is obtained by subtracting the average value of the map one resolution away from the point in question from the value of the map at the point of interest. In this procedure, the more slowly varying background is not deconvolved by the algorithm, but all sources with sizes of the order of the beam will be CLEANed. In addition to not modifying the background, this procedure converges very fast and a uniform level of CLEANing over the region being CLEANed can be achieved. This procedure has been successfully used in CLEANing our all-sky map. Even with a loop gain of 0.5 (usually considered high) we had no

difficulty with convergence. Compared to conventional CLEAN, this process showed a reduction in time by **atleast** a factor of

CLEANing **in** **practice** : (see tables 3.2 and 3.3) The dirty map (or the raw data) is available in files with each file having a size of 1 Hr x entire zenith angle range. Since the PSF has an extent of ±1 hour, we have to have the ±1 adjacent hours to CLEAN the central hour. To prevent the CLEAN procedure oscillating, the raw data has to be convolved in RA with a sinc function whose resolution in time corresponds to that of the EW array at 0° declination. This will smooth out amplitude scintillations on the map close to 0° dec. But the larger declination maps could still have some residual effects of scintillation; to remove those one should have used a sinc with a correspondingly lower resolution in time [in fact. lower by **cos(δ)]**. The reason to choose a sinc function appropriate for 0° declination is not to lose resolution on the map anywhere. There is no need for smoothing in declination since it is the direction of synthesis.
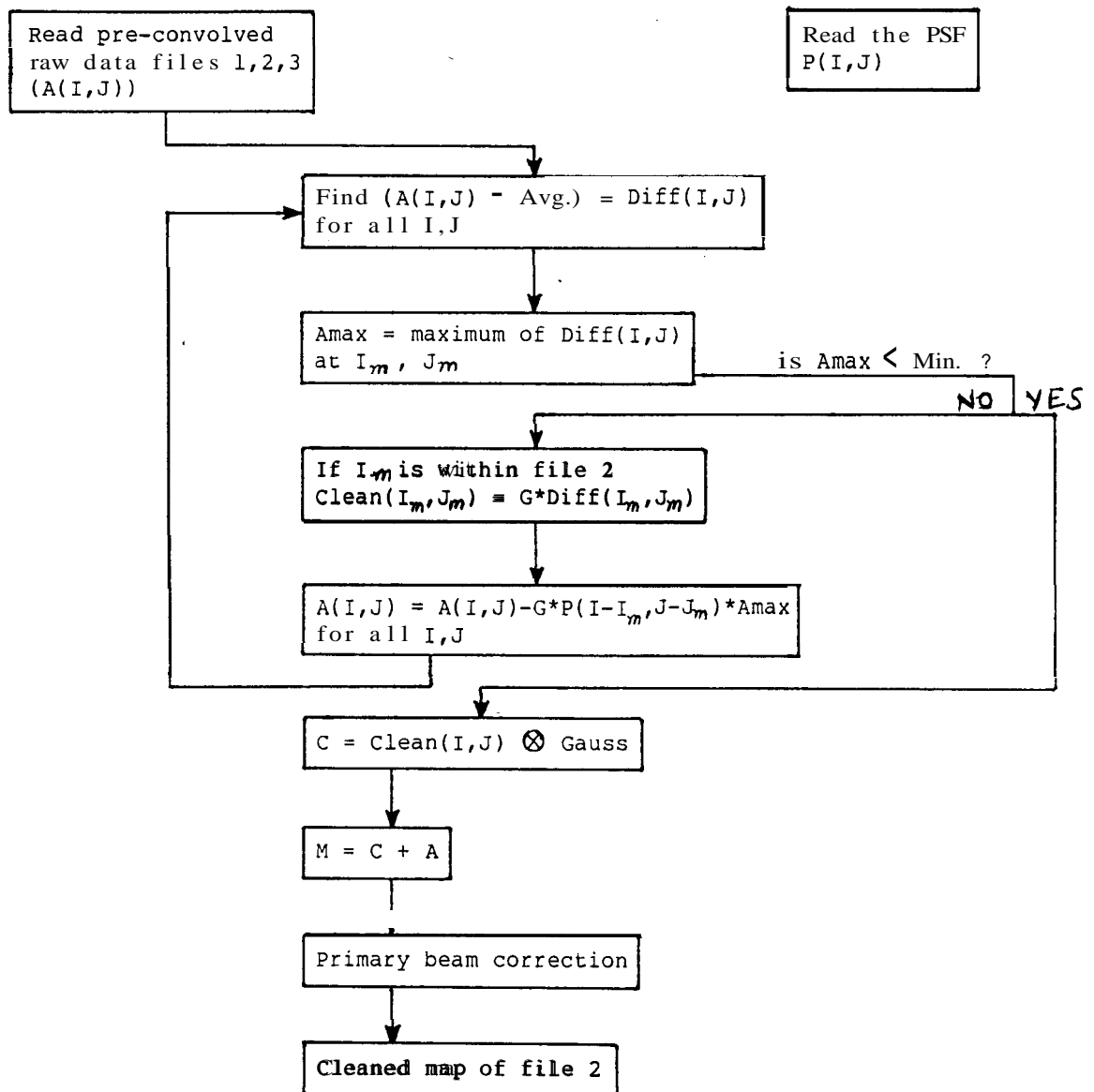
The PSF covers the entire zenith angle range in NS. The resolution of the PSF along NS does not change with its position in declination since both the PSF and the dirty map are in **sin(zenith** angle) coordinate system, but the PSF will have to be expanded or contracted along time depending on the declination of the source. In any one run of the program, only the central hour map gets **CLEANed.** The beam response due to any source in the 3 hour stretch(say, hours **1,2,3)** is removed but CLEAN components are written only if the source is located within the middle hour.

Table 3.2   Overall scheme to produce the final maps from the raw maps

```
                        ┌─────────────────────┐
                        │ Raw data files 1,2,3│
                        └─────────────────────┘
                                   │
                                   ▼
                        ┌─────────────────────┐
                        │ convolution to remove│
                        │ scintillations      │
                        └─────────────────────┘
                                   │
                                   ▼
                        ┌─────────────────────┐
                        │ Modified CLEAN      │
                        └─────────────────────┘
                                   │
            ┌──────────────────────┴──────────────────────┐
            ▼                                              ▼
    ┌───────────────┐                              ┌───────────────┐
    │ File 2.CLN    │                              │ File 2.RES    │
    └───────────────┘                              └───────────────┘
            │                                              │
            ▼                                              │
    ┌───────────────┐                                      │
    │ Convolve by   │                                      │
    │ Gaussian      │                                      │
    └───────────────┘                                      │
            │                                              │
            ▼                                              │
    ┌───────────────┐                                      │
    │ Make sure of  │                                      │
    │ normalisation │                                      │
    └───────────────┘                                      │
            └──────────────────────┬───────────────────────┘
                                   ▼
                        ┌─────────────────────┐
                        │ File 2.MAP          │
                        └─────────────────────┘
                                   │
                                   ▼
                        ┌─────────────────────┐
                        │ Primary beam factor │
                        └─────────────────────┘
                                   │
                        ┌─────────────────────┐
                        │ File 2.MAP          │
                        └─────────────────────┘
```

Table **3.3**   Modified CLEAN procedure adopted in the present work

---

Read pre-convolved
raw data files 1,2,3
(A(I,J))

Read the PSF
P(I,J)

Find (A(I,J) $-$ Avg.) = Diff(I,J)
for all I,J

Amax = maximum of Diff(I,J)
at I_m , J_m

is Amax $<$ Min. ?

NO   YES

If I_m is within file 2
Clean(I_m,J_m) = G*Diff(I_m,J_m)

A(I,J) = A(I,J)-G*P(I-I_m,J-J_m)*Amax
for all I,J

C = Clean(I,J) $\otimes$ Gauss

M = C + A

Primary beam correction

Cleaned map of file 2

This makes sure that the central hour is CLEANed of the sidelobes of any source sitting within an hour of it. Along NS however, the edges of the map in N and S are treated as though they are connected to each other. So, if the extent of the PSF overshoots any one edge, it continues on to the map from the other edge. In this sense **CLEANing** is done as though the map was on a cylinder, with the NS extent equal to the circumference of the cylinder. At the end of the run, the middle hour (in this case, hour 2) will be CLEANed. The next run can take dirty maps **2,3,4** and so on. The CLEAN components are convolved with a Gaussian whose area and the full widths at half maxima in the two perpendicular directions are the same as those of the PSF and then added to the residue map to obtain the final map. The area of a Gaussian of unit height whose full width at half maximum is the same as that of the PSF is greater than that of the PSF of unit height. Since the areas of the two are made equal the heights of the Gaussians and consequently of the sources that are CLEANed come down as compared to their heights in the dirty map.

It was possible to CLEAN the whole sky down to an almost uniform level 5 , where σ is the **r.m.**s. fluctuation on the dirty map. The **r.m.s.** value itself varies over different regions but not by more than a factor of 2. The next chapter contains more detailed discussion of the σ of the maps, residual sidelobes, dynamic range of the map, etc. There were, however, some complications near strong sources like Tau **A**, Vir A, Cas A and Cyg A. Since the template extent was only ± 1 hour, sidelobes beyond ± 1 hour from a source cannot be CLEANed in this process. So, while **CLEANing** regions around a strong source, the source may

not be in the field of analysis but its far off sidelobes will be. To avoid picking up the sidelobes as sources, these regions are flagged beforehand. While the sidelobes remain as they are in the final map, at least they will be restricted to a narrow range of declination around the source but wider range in RA and do not cause larger damage to the map.

CLEANing around Cas **A** was the most difficult since any **non-ideal** behaviour (though small in pecentage) leaves sidelobes which are large in absolute terms. The problems with Cas **A** are:

(a) Its flux is $\simeq 40000$ Jy which leads to large artefacts.

(b) Since it is at $\simeq 45^{\circ}$ zenith angle the effect of bandwidth decorrelation is more severe.

(c) Its **declination** is $\simeq 60^{\circ}$. The convolving beam is a **sinc** function whose resolution in RA corresponds to that at 0° dec.. Hence the effect of scintillations will not be reduced to as low a level as possible.

(d) Curved RA sidelobes leave a percentage of the peak as **unCLEANed** sidelobes which is still large in absolute terms.

(e) Significant strength of sidelobes even beyond one hour.

(f) Difference from the Cygnus PSF used for CLEANing.

Most of these problems can be taken care of if a special treatment is given to the maps around Cas **A**. In the maps presented in the next chapter this is **not** done. Special treatment to take care of problems (a) to **(f)** will be done in the future but are beyond the scope of this thesis. However, this does not affect the discussions given in the subsequent chapters.

3.2.4 Subtraction of additional offsets

The final maps produced showed several features which were suspected to be artefacts and not astronomical. These features were of the size of the synthesised beam in NS but continued for hours in EW!. With a view to understanding this problem, and correcting it, the following analysis was done. The residue map of one hour in extent was averaged along time to produce one profile along declination - for a given declination, the values in the residue map were summed along time and all points beyond 5σ are not considered for averaging to remove any source contribution. Obtaining one average value for each declination, we get a profile in declination but which is the result of averaging for one hour in time. This can be fourier transformed and the resulting pattern of the amplitude of correlations can be studied. Fig. **3.15** shows one set of patterns for the averaging done from $06^h 30^m$ to $07^h 30^m$. The higher values of amplitude seen in the first few short spacings (< 50 **m)** is understandable as the residue map contains the smoothly varying sky which will reflect in higher values of correlations seen in shorter spacings. On the other hand, the residue map does not contain any strong point source. The contributions of the weaker point sources will be heavily suppressed since the averaging is done for an hour. In addition, all points beyond 5σ **have** not been included in the summation which means most of the weaker sources have also been excluded in the summation. Now if one looks at the amplitude of correlations in the longer baselines, its value is not expected to be more than the noise one can estimate for an averaging of 1 hour of data. The **r.m.s.** on each sample on the
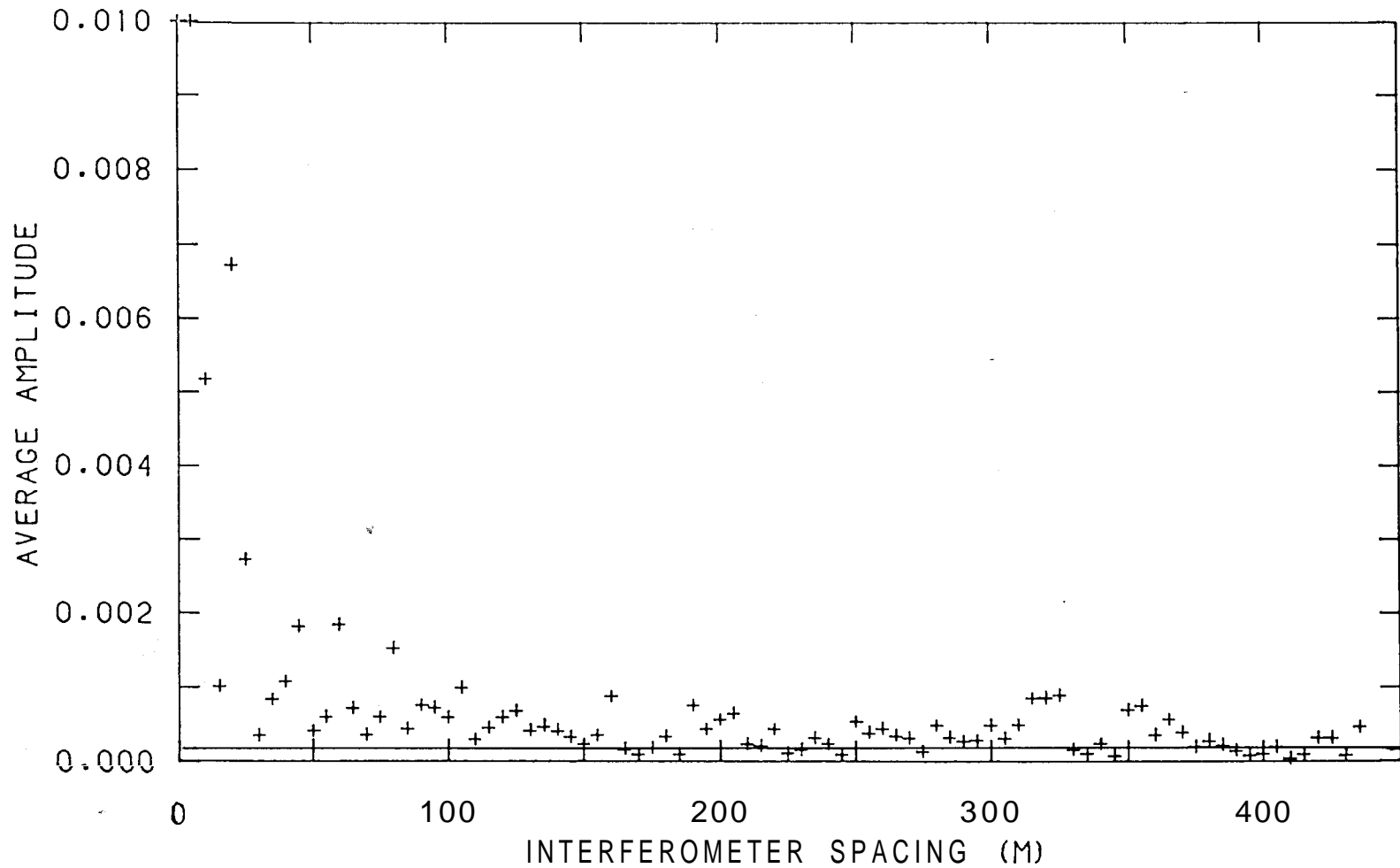
Fig. 3.15: One hour average of correlations. The averaging was done from 06^h30^m to 07^h30^m. Notice many values in the longer baselines which are beyond 3σ (solid line). These values produce artefacts in the map which are narrow in declination but continue for long length of time. The higher values in the shorter spacings are due to the presence of the sky contribution in them.
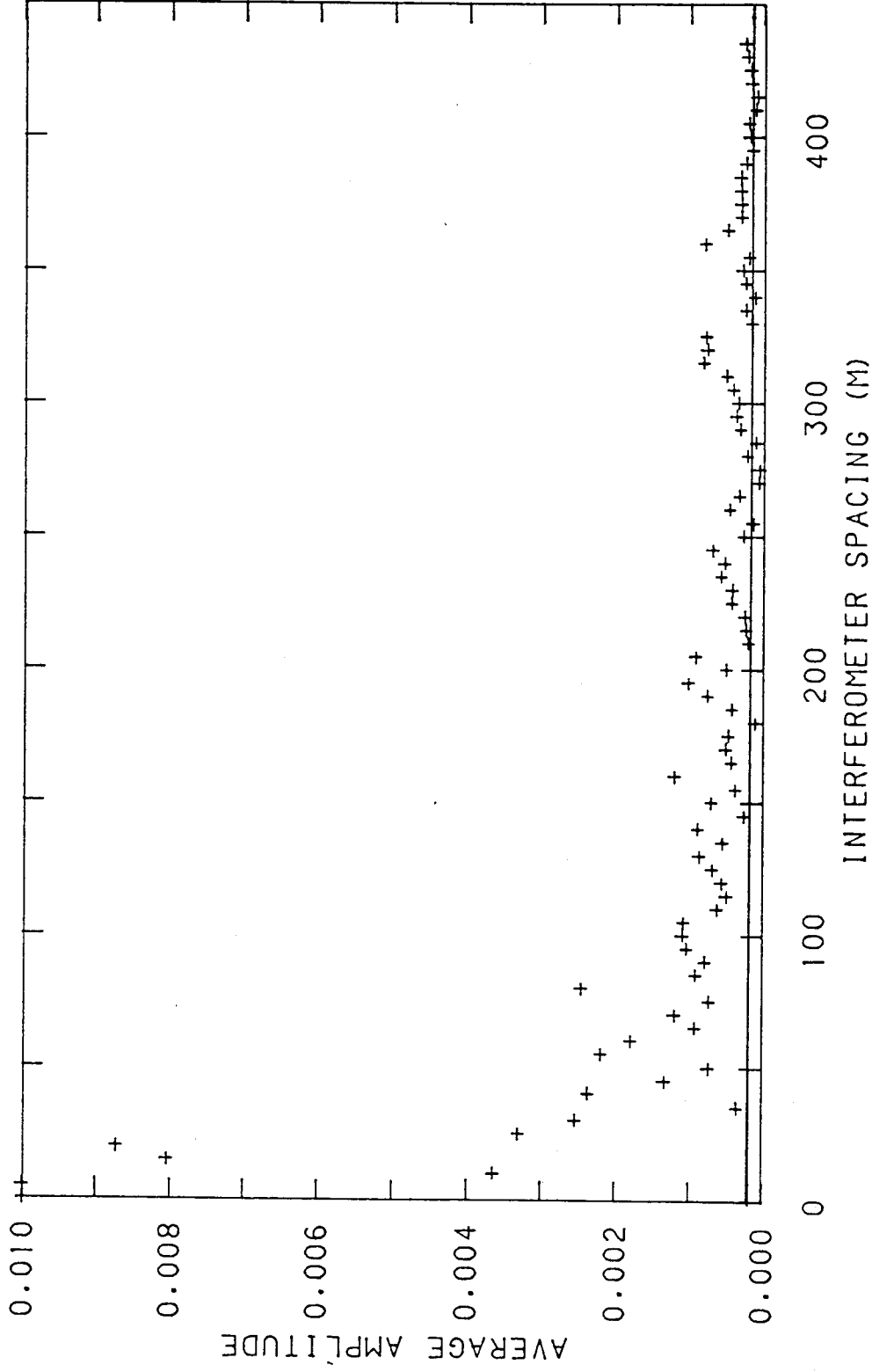
Fig. 3.16: Same as Fig. 3.15 but for the averaging between 16^h30^m and 17^h30^m. Notice the similarity of the pattern in the longer baselines as compared to that in Fig. 3.15.

map $= 1/\sqrt{Bt} = 6\text{x}10^{-4}$ for B = 400 KHz and t = 6 sec. There are 143 independent samples in an hour and hence the **r.m.s.** on any **1** hour averaged correlation $\approx 0.5\text{x}10^{-4}$. The corresponding **r.m.s.** value on the amplitude of correlations will be $\sqrt{2}\text{x}0.5\text{x}10^{-4}$. The line drawn indicates the 3σ level. Most of the amplitudes in the long baseline interferometers are beyond 3σ. To convince ourselves that these offsets exist at all times the data for each hour was averaged and 24 sets of profiles obtained. As a sample, Fig. **3.16** shows the averaging from $16^h\ 30^m$ to $17^h\ 30^m$. There is considerable similarity in the long baseline patterns, considering that two far-removed hours have been averaged. The origin of these offsets is not completely clear but we are reasonably sure that it is coming from outside the receiver. However, a remedy to this problem is to subtract the long baseline (>50 **m**) offsets from the data. It turns out that subtraction of one offset profile for the entire 24 hours does not take care of this problem completely but what is most appropriate is to subtract a moving one hour average from the data. Considering the way the offsets are obtained and that subtraction of offsets is done for only those spacings which are greater than **50** m, there is very little modification, if any, of the sky. Of course, it can also be verified by looking at the maps produced with and without the offsets and making sure that only the non-physical narrow features have disappeared.

3.3 CALIBRATION

3.3.1 Cygnus A as calibrator

The data in the final map after CLEAN will be in arbitrary

units and for further interpretation and analysis it should be calibrated against **Jy/beam** or, equivalently, in brightness temperature units. Cyg A was chosen as a calibrator for this purpose. Absolute flux density measurements of Cyg **A** are available from **10** MHz to **22 GHz** (Baars et al. 1977). At frequencies around **30** MHz its absolute flux is known to within   . **5%.** The present maps have been calibrated against the ebsolute flux density of Cyg A which is taken to be **25396** Jy at **34.5** MHz obtained by using the spectral fit given by Baars et **al.(1977).**

3.3.2 Estimating fluxes of sources

Estimating fluxes of sources in the presence of background is not straight forward. In the simplest scheme, one can simply locate the peak of the source and the value of the local background and the difference would give the flux. This would be accurate provided,

(a) the source is a point source (size << size of beam)

(b) the sampling of data is fine enough to locate the peak **properly,and**

(c) there are no scintillations.

In general, however, none of these need be true. An alternative method would be to estimate the integrated value of the map within the size of the source(main beam, if it is a point source). While this takes care of the points(a), (b) and(c) mentioned above, the summation becomes sensitive to the determination of the average value of the background which has to be subtracted from every point summed over the size of the source,

One way to avoid this problem is to remove the background by a filter. Consider convolving the map in both the dimensions (RA and Dec.) by a function of the form shown in Fig. **3.17.** This will essentially filter off all brightness variations in the map with angular scales larger than the separation between the negative delta functions. A special case of this method has been adopted by Williams et al. **(1966)** to obtain the fluxes of' point sources. The map left after convolution can simply be summed within the size of the source to obtain the integrated flux from the source. This method has been successfully adopted to obtain fluxes of both point sources and extended sources in the present survey.

3.3.3 The flux scale

We checked to see whether the flux scale

(a) is independent of the strength of the source and,

(b) whether there are any systematic patterns as a function of RA or declination.

For this purpose, the results from the survey at **38** MHz (Williams et al. **1966)** were made use of. Kellermann et al. **(1969)** list the **38** MHz fluxes for most of the **3C** sources, This list contains **21** Ⓐ sources for which the estimated standard error is **5%** and **118** Ⓑ sources for which the estimated standard error is between **5%** and 15%. A percentage difference between the two flux estimates of each of these two types of sources was obtained as follows:

$$\% \text{ error} = \frac{\text{Flux at 38MHz} - \text{Flux at 34.5MHz}}{\text{Flux at 38 MHz}} \qquad (3.10)$$
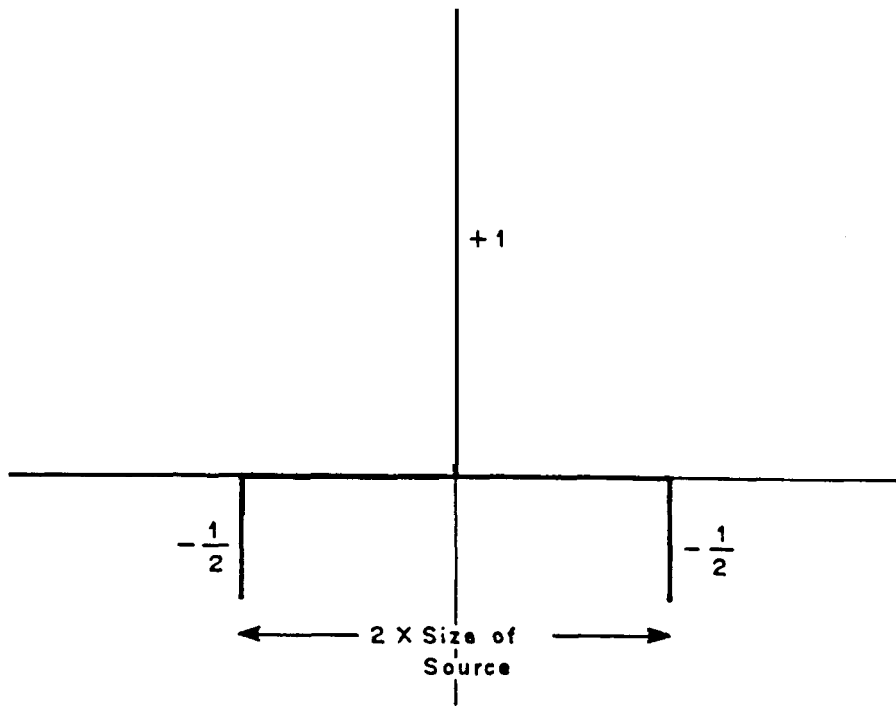
Fig. 3.17:   Convolving function used to filter the background.

This percentage error is plotted against RA, dec. and flux to see if there is any systematic pattern. This can, of course, be meaningfully done only on the Ⓑ sources since they are ≈ 100 in number and the statistics is better.

Figure 3.18 shows a plot of this percentage error against the declination of the 82 of Ⓑ sources. The Ⓑ sources left out are those which are weak ($\lesssim$ 30 Jy) or at high declination ($\gtrsim 70^{o}$) as well as those which fall well beyond 3σ of the distribution. Their inclusion will only introduce unwanted noise. A sloping trend is clearly seen. It is extremely unlikely that any of our antenna based effects are monotonic in dec. from -2° to $+60^{o}$ when the instrumental zenith is at $+14^{o}.1.$ A clue to understanding this pattern comes from the fact that the 38 MHz survey is made up of two surveys one centered at $+7^{o}$ and the other at $+52^{o}$ with the full width at half maximum of the EW antenna pattern being $47^{o}.$ Thus the source list is made up of two sets of sources with their declinations being less than or greater than $+30^{o}$ (see Williams et al. 1966 and Fig. 6 in it). So, we have calculated the average and r.m.s. value of the percentage error in the two zones : $< 30^{o}$ and $> 30^{o}$. The results are as follows :

$$\text{(average)} \quad \textbf{(r.m.s.)}$$

for sources with $6 < 30^{o}$, % error = 9.5 ± 18 (52)

$\qquad\qquad 6 > 30^{o}$, % error = −0.5 ± 14 (30)

where the numbers in brackets indicate the number of sources in the two zones. Thus, there appears to be a 10% difference in the average calibration of the fluxes of the two sets of sources in the 38 MHz survey of Williams et al. (1966).

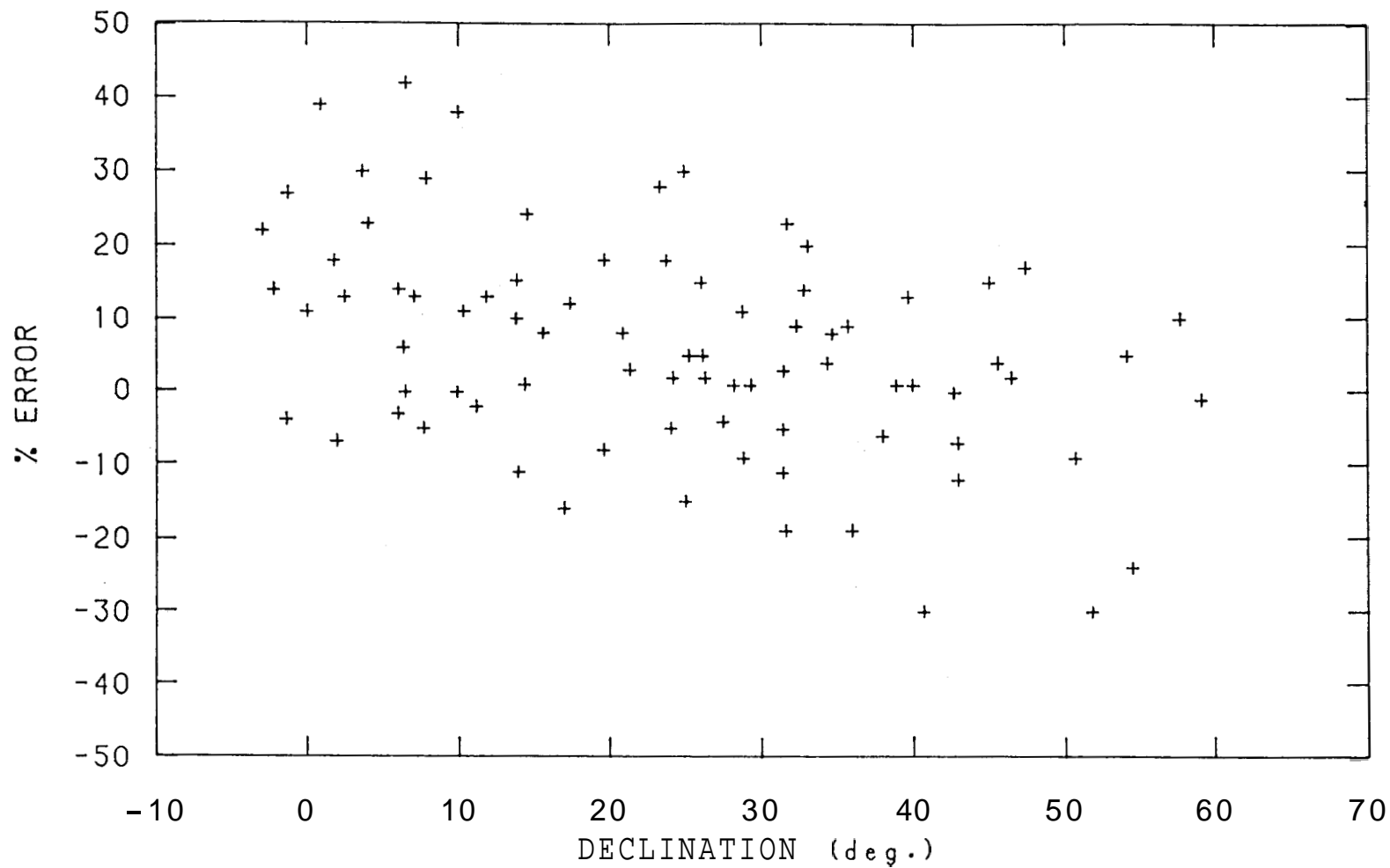Figure 3.19 shows the same plot as Fig. 3.18 but with the

Fig. 3.18: Percentage difference between the fluxes of some 3C sources at 34.5 **MHz** and at 38 **MHz** plotted as a function of the declination of the sources. The slope is probably due to the difference in the flux calibration of the 3C sources at 38 **MHz** depending on whether they are below or above +30° declination.
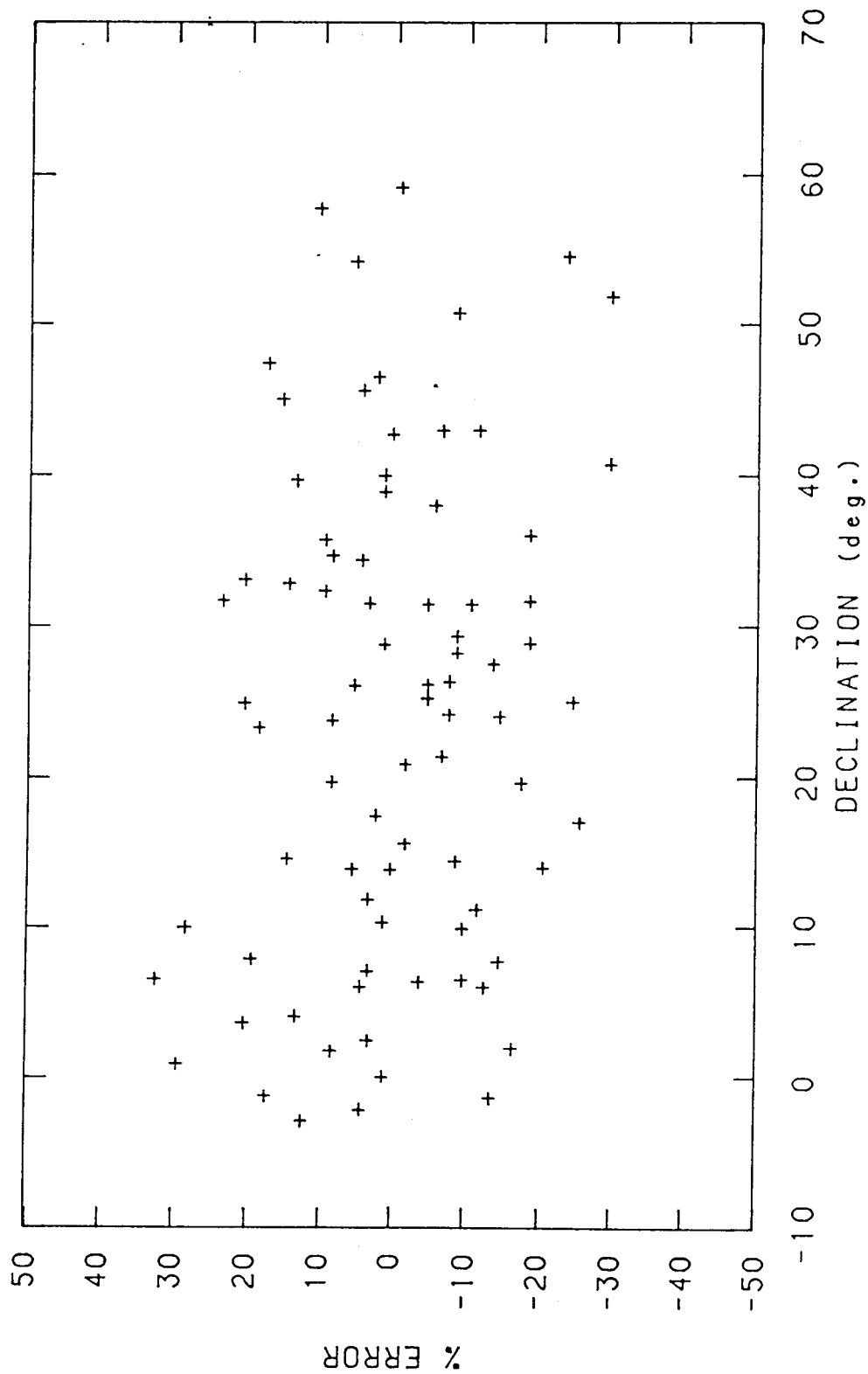
Fig. 3.19: Percentage difference between the fluxes as in Fig. 3.18 but the average calibration difference in the fluxes at 38 MHz between the sources below and above +30° dec. has been corrected. The systematic pattern seen in Fig. 3.18 is much less evident here.
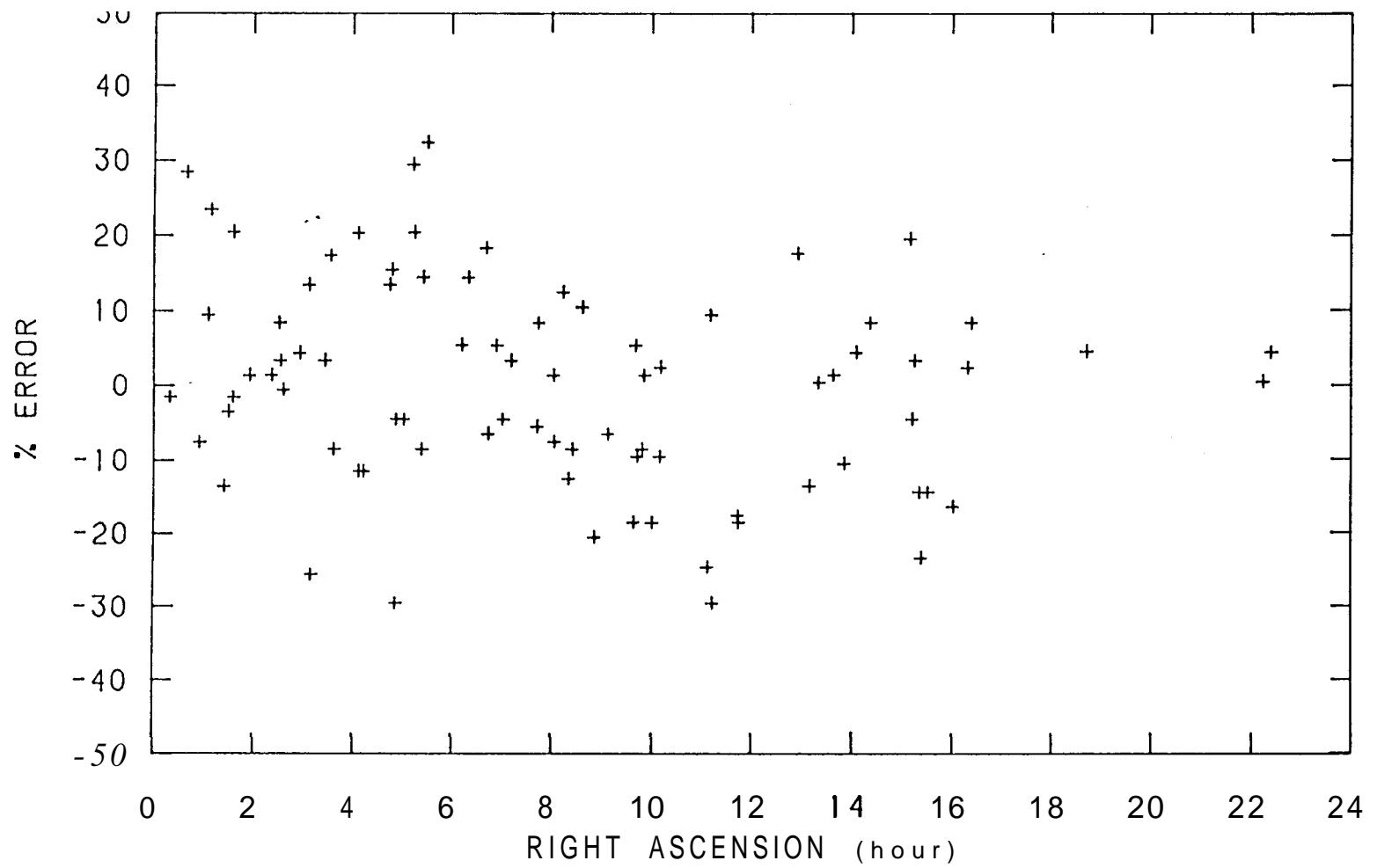
Fig. 3.20: Same as Fig. 3.19 but plotted against R.A.. No systematic pattern is evident here.
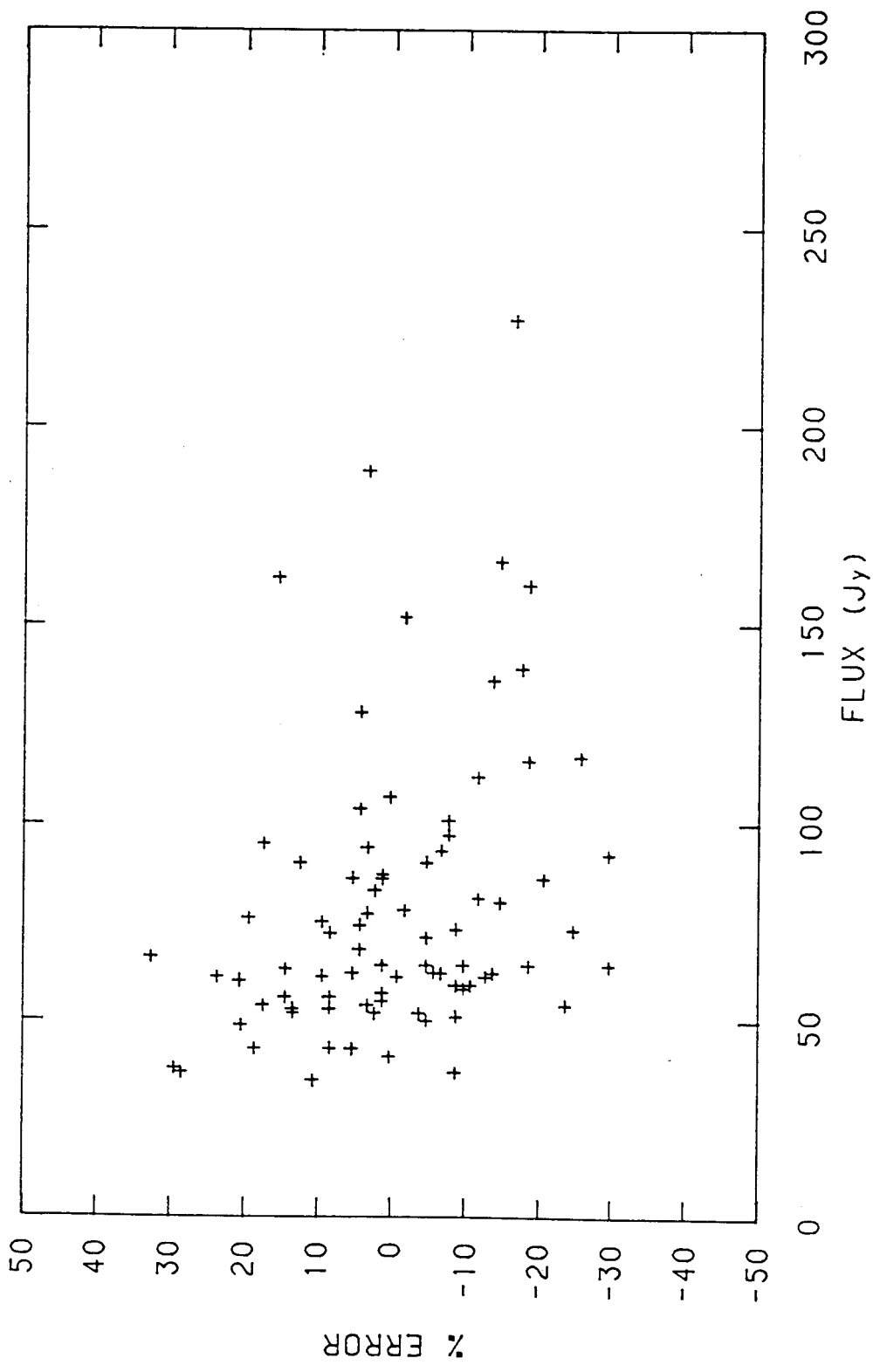
Fig. 3.21: Same as Fig. 3.19 but plotted against flux to look for any non-linearity in the flux scale. None is apparent.

offset adjusted at $+30^{\circ}$. The slope is much less apparent. Figures 3.20 and 3.21 show similar plots against RA and flux. There is no apparent systematic pattern in these. Taking an average value for the **r.m.s.** of the percentage error between the twp fluxes (i.e. 38 MHz and **34.5** MHz) to be 16%, and the **r.m.s.** value of the percentage error in the 38 MHz flux to be **10%,** an error of 12% is implied in the fluxes at **34.5 MHz.**

For the (A) sources the results are as follows:

(average) **(r.m.s.)**

for sources with $\delta < 30^{\circ}$, % error = 0.63 $\pm$ 4 (8)

$\delta > 30^{\circ}$, % error = 5.4 $\pm$ 8 (10)

Due to the small numbers involved it is difficult to comment on the statistical significance of the difference in the averages. In any case, the average of the two **r.m.s.** values on the percentage error of 6% implies an **r.m.s.** value for (A) source fluxes at **34.5** MHz of < **5%.**

It is interesting at this stage to draw attention to Fig. **3.22.** Here, the percentage error **for** (A) sources are plotted against declination. However, the **34.5 MHz** fluxes were deliberately not corrected for the primary beam effect. A 3rd order polynomial fit to the pattern is shown by the solid curve. This curve is very close to the square of the pattern written in equation 2.1. Assuming that there are no systematic patterns in the 38 **MHz** fluxes of the (A) sources, this can be taken as a 'verification' of the primary beam pattern of the basic dipole in its perpendicular plane.
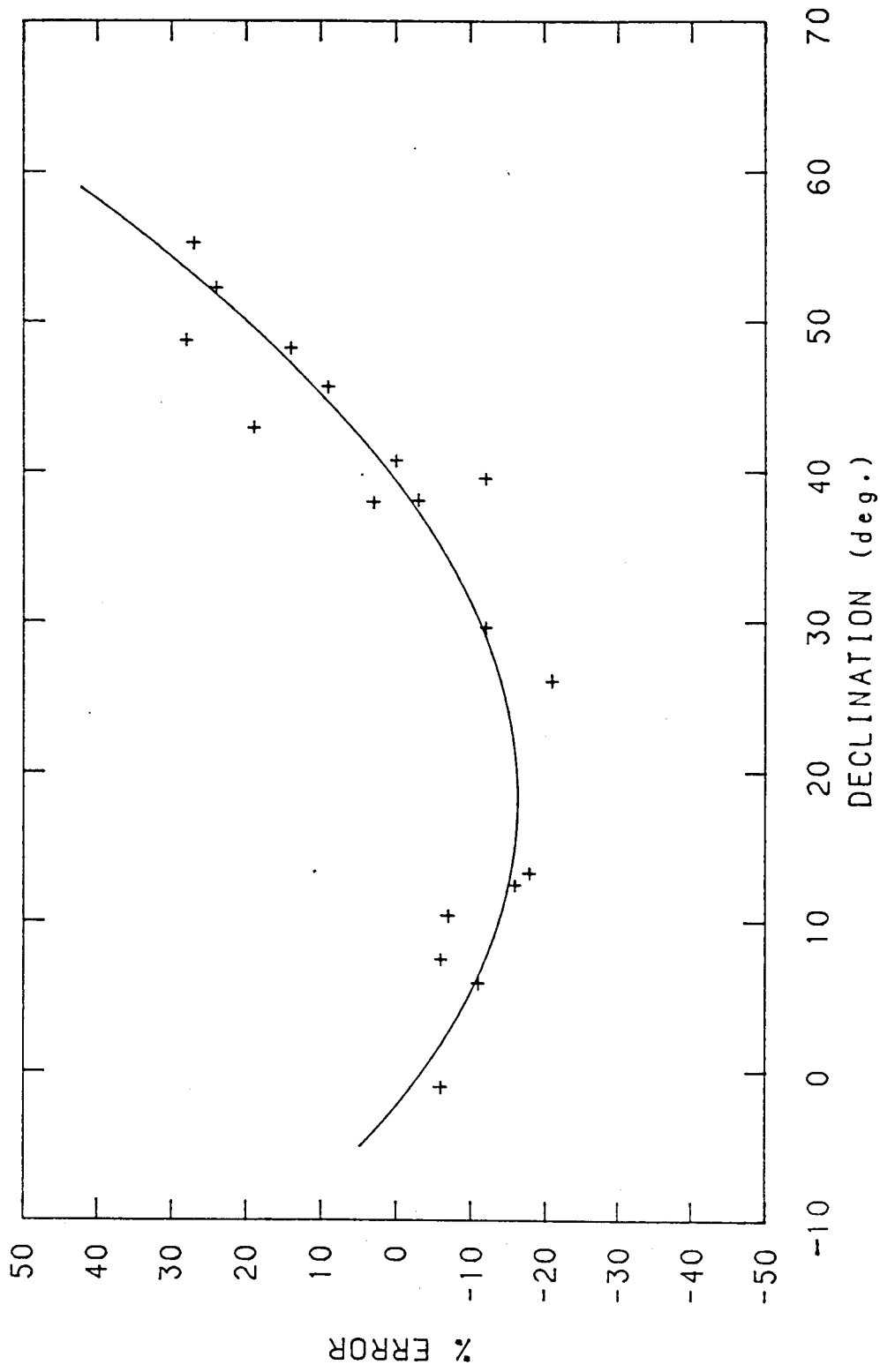
Fig. 3.22:   Verification' of the primary beam pattern

3.3.4   Repeatability

It is important to check the repeatability of the 34.5 MHz observations as interference and ionosphere can affect the data in addition to system variation.   With this purpose in mind, the fluxes of all the ⒷB sources were estimated on another day's observation, and the differences in the fluxes between the two days found out. They agree to within 8% (**r.m.s.** value).

3.3.5 Calibrating the map to brightness temperature

It is useful in many contexts to talk of the equivalent black body temperature or the brightness temperature of the radiation observed, even though the source may not be a black body. The brightness temperature is related to the flux through the Rayleigh-Jeans formula (an approximation valid at radio wavelengths) as follows:

$$S = \frac{2k_B}{\lambda^2} \int T_B \, d\Omega \qquad (3.11)$$

where,

S   is the flux observed,

k_B is Boltzmann's constant,

A   is the wavelength of observation,

T_B is the equivalent black body temperature, and

$d\Omega$ is the solid angle from which the radiation is coming.

.   Consider now the diffuse background. What we **observe(S)** is the result of convolving this with the antenna beam.   To associate a brightness temperature to this background emission we have to obtain the solid angle of the antenna response. This can be done by integrating the PSF that has been used for **CLEANing**

the maps.   Again considering Cyg A whose flux density (S) we know, an integration of the PSF gives us the conversion factor from **Jy/beam** to K,   through equation 3.11.   This analysis gives 1 **Jy/beam** : 436 K.   This is what is commonly referred to as the full beam brigtness temperature.   This conversion has been used in the maps to give the background an equivalent black body temperature.

APPENDIX 1

CURVATURE OF R.A. SIDELOBES

This arises due to the fact that the source goes through different NS beams of the telescope at different hour angles. When the source is at transit, its response is at say δ_1 the declination of the source. As the hour angle of the source becomes different from zero the response of the source will be at a more positive declination (if the telescope is situated at positive latitudes) as can be seen in the figure (Fig. 3.A1.1). As seen on the maps, the apparent zenith angle of the source changes resulting in the curved R.A. sidelobes (Fig. 3.A1.2). This change can be calculated through the following relation:

$$m = \cos\delta \cos H \sin\phi - \sin\delta \cos\phi$$

where,

q = sine of zenith angle of the source as measured on the **map**,

δ = declination of the source,

H = hour angle of the source, and

ϕ = instrumental zenith.

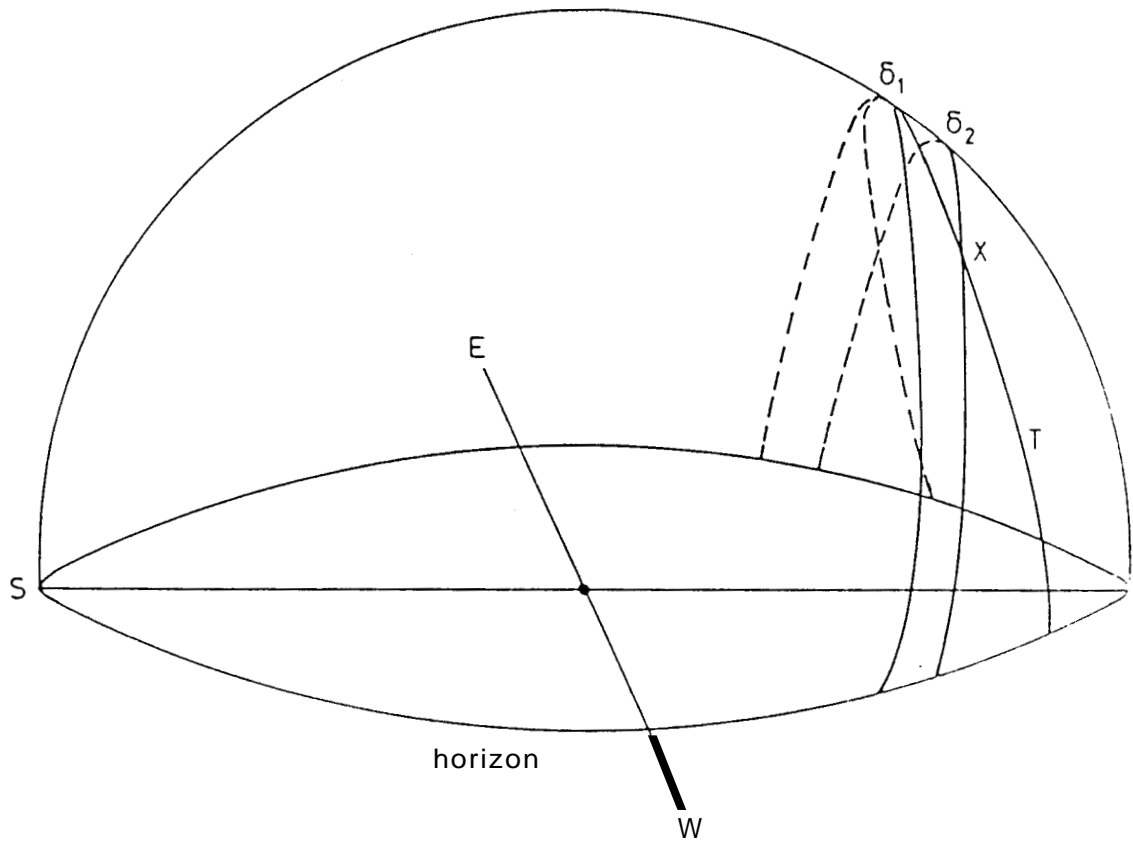This effect would not be there if we were at the equator.

Fig. 3.A1.1: This illustrates the origin of the curved RA sidelobes. The response of the array will be in a plane perpendicular to the horizon as shown corresponding to two decs. δ_1 and δ_2. A source at dec. δ_1 moves in a track (T) tilted at an angle to this. This angle is equal to the latitude of the array. So, at an hour angle corresponding to X, the reponse of the array to the source will be at δ_2. If we were at the equator, T would have been the same as the curve drawn at δ_1
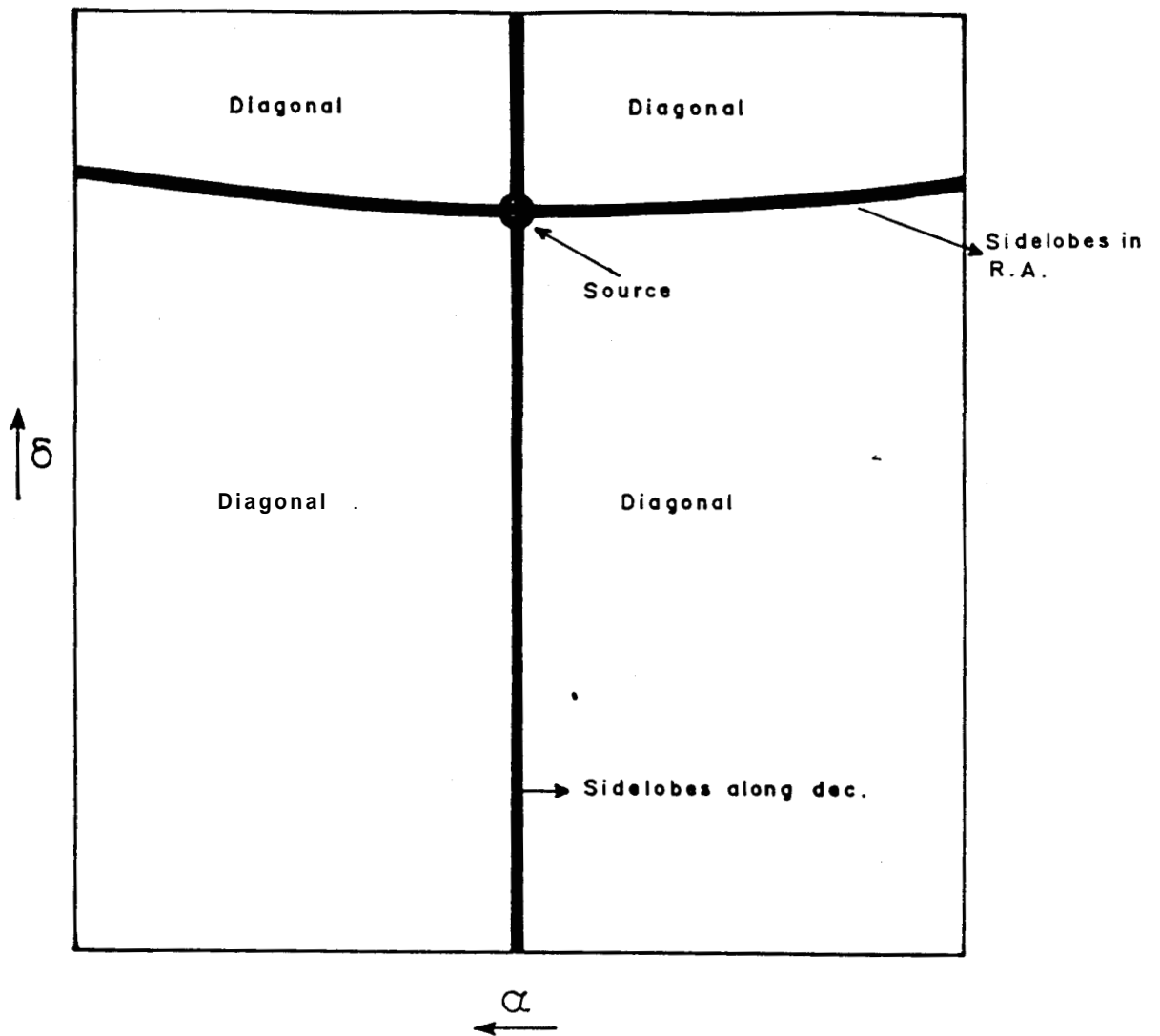
Fig. 3.A1.2:   Curvature of the RA sidelobes of a source as seen on the map indicated schematically.   Due to this curvature, the PSF cannot be estimated very accurately in the scheme adopted by us.   This leads to residual sidelobes even after CLEANing.   The residue left is maximum along the darkened patch (along the "+") and decreases as one moves along the diagonal.

REFERENCES

Abramowitz, M., Stegun, I.A. , Eds. Handbook of Mathematical
 Functions, New York, Dover Publications Inc.

Baars, J.W.M., Genzel, R., Pauliny-Toth, I.I.K., Witzel, A. 1977,
 Astron. Astrophys,, **61,** 99.

Christiansen, W.N., Hogbom, J.A., 'Radio telescopes', Cambridge
 University Press, 1985.

Hogbom, J. 1974, Astrophys. J. Suppl. 15, 417.

Kellermann, K.I., Pauliny-Toth, I.I.K., Williams, P.J.S. 1969,
 Astrophys. J., **157,** 1.

Wakker,B.P., Schwarz, U.J. 1988, Astr. Astrophys., 200,312.

Williams, P.J.S., Kenderdine, S., **Baldwin,** J.E. 1966,
 Mem. R. Astr. Soc., 70, 53.